Politecnico di Milano

SCHOOL OF INDUSTRIAL AND INFORMATION ENGINEERING

Master of Science – Nanotechnology and Material Engineering

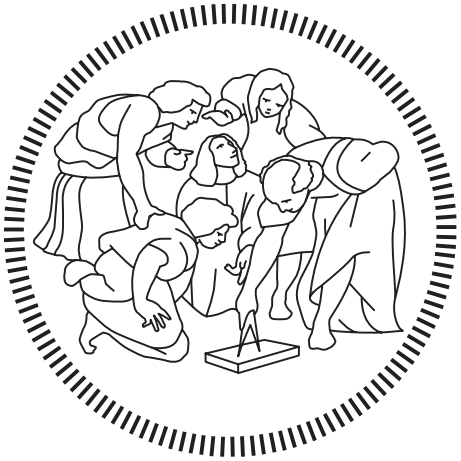

A High-Performance Nanostructured Carbon Electrode for Vanadium Redox Flow Battery

Supervisor

Prof. Matteo ZAGO

Co-Supervisor

PhD. Fabio DI FONZO

Candidate

Simone FIORINI GRANIERI 10602226

Academic Year 2019 – 2020

THIS PAGE IS INTENTIONALLY LEFT BLANK

Table Of Contents

List Of Figure

List of tables

Abstract

Vanadium redox flow batteries are one of the most promising electrochemical energy storage systems on the market today, thanks to the peculiarity of decouple energy capacity and deliver power. The low power density is the main weak point, it is due to the use of electrodes not optimized for this purpose, with high electrical conductivity but with a low surface area and an electrochemical activity not specific for vanadium redox reaction.

For this purpose, a nanostructured carbonaceous material was deposited on gas diffusion layer (GDL) of carbon paper 39AA Sigracet, through a novel deposition technique, with the aim of increasing the surface area available to the reaction, without affecting the permeability and diffusion of the electrolyte and without lowering the electrical conductivity. The electrode thus formed has been heated up to 1100 ° C in high vacuum, during the heat treatment it was noted an increase in the degree of graphitization and electrical conductivity, as well as the formation of carbon allotropes such as fullerenes and carbon nano-onion. The development of a characterization procedure, which includes microscopy techniques (SEM) and spectroscopy (XPS, Raman), allowed to verify the physico-chemical properties of the material and to correlate the deposition parameters on the observed properties, also predicting how these affect the electrochemical activity, moreover through the use of XPS spectroscopy it was possible to evaluate the presence of contaminants such as nitrogen and oxygen, present with a relative concentration around 2% for both atoms, their concentration decreases as the annealing temperature increases, meanwhile an increasing on carbon allotropes relative concentration is faced. To test the performance of the electrode, electrochemical tests were carried out in order to study kinetics and mass transport phenomena. Specifically, cycle voltammetry tests, polarization in a symmetrical cell and tests on a segmented full cell using a Nafion 115 membrane and a serpentine flow field which proved to be the most suitable with this type of GDL. The analysis was focused on the anode since it is believed that it is the limiting electrode of the battery. Through the CV it was possible to analyze which heat treatment leads to the best kinetics towards the oxidation reaction of Vanadium, which was found to be at 1000 ° C, with a spread of 100mV and a ratio between oxidation peak and reduction of 0.9 . From tests in symmetrical cell which was carried out varying the electrolyte distributor (flow field) and flux at SOC 50%, it was possible to calculate an electrode over potential of 60mV for a current density of 400mA/cm^2. The tests in the complete cell were conducted at different current densities, so

to analyze the variation of the energy, voltaic and coulombic efficiency values, the analyzed current densities are: 100, 200, 300, 350, 400 mA / cm2 and the following voltages efficiency results were obtained respectively 96.2%, 93.9%, 91.2% 89%, 88.1%, the following values were calculated by eliminating the contribution of the membrane over potential (iR correction).

The use of the nanostructured graphite electrode with the presence of carbon allotropes such as fullerenes and nano-onion has led to an improvement in the generic cell efficiency of about 20% compared to the commercial version, with an energy efficiency of 91.3% , 88.3%, 90.2%, 87.8% for current density of 100, 200, 300, 350 mA / cm2 respectively.

It was therefore argued that, although the presence of carbon bonded atoms such as nitrogen and oxygen is effective in improving the performance of the electrode, the greatest contribution is given by the presence of carbon allotropes increasing drastically the active sites for the redox reaction of Vanadium.

Sommario

Le batterie a flusso al vanadio costituiscono uno dei sistemi elettrochimici di stoccaggio energetico tra i più promettenti oggi sul mercato, soprattutto grazie alla peculiarità di poter disaccoppiare capacità energetica e potenza. La bassa densità di potenza è il principale punto debole, essa è dovuta all'utilizzo di elettrodi non ottimizzati per tale scopo, dotati di alta conducibilità elettrica ma con attività elettrochimica non specifica verso gli ioni vanadio e con bassa area superficiale.

A questo scopo è stato depositato su gas diffusion layer (GDL) di carbon paper 39AA Sigracet, attraverso una tecnica di deposizione sperimentale, un materiale carbonioso nanostrutturato con il fine di aumentare l'area superficiale disponibile alla reazione, senza influenzare la permeabilità e la diffusione dell'elettrolita e senza abbassare la conducibilità elettrica. L'elettrodo così formato ha subito un riscaldamento fino a 1100°C in alto vuoto, durante il trattamento termico si è notata un aumento del grado di grafitizzazione e della conduttività elettrica, oltre che alla formazione di allotropi del carbonio come fullereni e carbo nano-onion. L'elaborazione di una procedura di caratterizzazione, che comprende tecniche di microscopia (SEM, TEM) e spettroscopia (XPS, Raman), ha consentito di verificare le proprietà fisico-chimiche del materiale e correlare i parametri di deposizione sulle proprietà osservate, pronosticando anche come queste influiscano sull'attività elettrochimica, inoltre attraverso l'uso della spettroscopia XPS è stato possibile valutare la presenza di contaminanti come azoto e ossigeno, presenti con una concentrazione relativa che si attesta attorno al 2% per entrambi gli atomi, la loro concentrazione diminuisce all'aumentare della temperatura di annealing, mentre si ha un aumento della concentrazione relativa di allotropi del carboni. Per testare la performance dell'elettrodo sono state effettuate delle prove elettrochimiche così da studiare fenomeni di cinetica e di trasporto di massa. Nello specifico sono state effettuate delle prove ciclo voltmetriche, delle prove in cella simmetrica variando il distributore di elettrolita (flow field) e la velocità di flusso, ed infine dei test su cella totale segmentata, utilizzando una membrana Nafion 115 e un flow field a serpentina che si è dimostrata essere il più adatto con questa tipologia di GDL. Si è focalizzata l'analisi sull'anodo poiché si ritiene che esso sia l'elettrodo limitante della batteria. Attraverso la CV si è potuto analizzare quale trattamento termico porti alla migliore cinetica verso la reazione di ossiriduzione del Vanadio, che si è trovato essere a 1000°C, con uno spread di 100mV e un rapporto tra picco di ossidazione e riduzione di 0,9. Dai test in

cella simmetrica, con SOC al 50%, si è riusciti a calcolare un sovra potenziale dell'elettrodo di 60mV per una densità di corrente di 400mA/cm^2. I test in cella completa sono stati condotti a diverse densità di corrente, così da analizzarne la variazione dei valori di efficienza energetica, voltaica e coulombica, le densità di corrente analizzate sono: 100, 200, 300, 350, 400 mA/cm^2 e si sono ottenuti rispettivamente i seguenti risultati di efficienza voltaica 96,2%, 93,9%, 91,2% 89%, 88,1%, i seguenti valori sono stati calcolati eliminando il contributo di sovra potenziale dovuto alla membrana.

L'utilizzo dell'elettrodo grafitico nanostrutturato con presenza di allotropi del carbonio come fullereni e carbo nano-onion ha portato ad un miglioramento dell'efficienza generica di cella del 20% circa rispetto alla versione commerciale, con una efficienza energetica di 91,3%, 88,3%, 90,2%, 87,8% per densità di corrente rispettivamente di 100, 200, 300, 350 mA/cm^2.

Si è quindi affermato che, sebbene la presenza di atomi legati al carbonio come azoto e ossigeno sia efficace nel migliorare le prestazioni dell'elettrodo, il maggior contributo viene dato dalla presenza di allotropi del carbonio e di siti attivi per la reazione di ossidoriduzione del Vanadio.

Chapter 1
Introduction

1.1 Energy Storage Systems

In a scenario where global warming and environmental pollution are going to have a big impact on everyday life, a radical change on the usage and production of energy. Countries in the world, and especially in Europe, are working for changing their way to produce energy, from fossil fuel to renewable energy such as solar and wind source etc. The key to this change are systems for energy storage (ESS). In fact, renewable energy sources are intermittent and unpredictable on the long time span, hence, it is not possible to use them by their own to guarantee a constant supply of energy. In this respect EES allow to store and provide energy as needed, playing an important role to overcome renewable energy issues European parliament is taking seriously this progress, and is focusing its economic and energetic growth in this way, in fact it has established an agreement (Europe 2050) to reach a zero impact on global warming in 2050 [1]. Among various energy storage technologies, redox flow batteries (RFBs) seem to be an ideal storage technology for wind and solar electricity because of their perfect combination of design flexibility, long cycle life, high efficiency and high safety [2]. In RFB energy is stored in fluid electrolyte solutions which are charged/discharged through electrochemical flow cells and stored in external tanks. The energy capacity of the system scales with the volume of tanks, whilst the rated power is determined by the electrode area, the possibility of decouple the capacity and the power permit the possibility of a scale-up of this technology in the stationary storage scenario [3].

1.2 Basic Principle Of An EES:

1.2.1 Cell Potential

A battery is an energy storage system that use chemical energy to convert in electric energy, it is made by two semi-cell, each compose by an electrode, responsible for the reaction, and an electrolyte, responsible of the ionic conductance. The two semi-cells are connected by a membrane that permit the protonic passage.

During the discharge process on the negative electrode, called anode, a reaction of oxidation happen, this reaction promote an electrons able to power an external load and recombine in the positive electrode, cathode, through a reduction reaction, where the charge carrier are released to pass through the electrolyte and the separator to the negative. The driving force for the electrons passage is the difference in Gibbs free force of the two reactions occurring at the electrode-electrolyte interface.

On charge process, an external load is applied to overcome the natural moving of electrons, converting electric energy into chemical energy, in this case we have reduction on the negative electrode and oxidation on the positive.

The reaction happens at the interface between electrode and electrolyte and the driving force is the potential difference on the two side, knowing as double layer, the cell's potential is the sum of the interface potential between negative and positive electrodes. Cell voltage is associated to the free Gibb's energy and can be thermodynamically calculated by the Nernst equation.

Considering a generic redox reaction:

$$A + e^{-} \leftrightarrow B$$

The free Gibb's energy can be calculated in this way:

$$\Delta G_{electrode} = \Delta G^{0} + RTln(K_{electrode}) = \Delta G^{0} \ln\left(\frac{a_{product}}{a_{reactant}}\right)$$

Knowing

$$\Delta G = -nFE$$

We obtain the equation

$$E = E^0_{electrode} - \frac{RT}{nF}\ln\left(\frac{a_{producct}}{a_{reactant}}\right)$$

This equation is applicable to the single electrode per single reaction. The cell voltage is the difference between the energy of the electrodes

$$\Delta V = E_{cathode} - E_{anode} = E_{cell}$$

From those equation is straight that the cell voltage depends on the activity of the chemical species. So, it would not be constant during the work of the battery.

1.2.2 Effective Potential

The theoretical voltage of an EES is based on the electrochemistry of a thermodynamic equilibrium. Actually, the work potential of the cell is different from the theoretical one in standard condition.

This deviation is called overpotential, and is defined as:

$$\eta = E - E^0$$

The intensity of this deviation is influenced by several factor as: electrode geometry, composition, concentration of electrolyte, cell architecture and temperature. The electrochemical reaction, happening on the electrode-electrolyte interface, follow different steps:

- Mass transport of reactant from the bulk solution to the interface of electrode
- Adsorbiment of the chemical species on the electrode surface
- Effective reaction between adsorb species, with charge transfer
- Desorbiment of the product
- Mass transport of the product from the surface to the bulk solution

On those steps, the slowest is the one that determine the reaction velocity, the rate determining step [4]. The overpotential can be divide in three type of overpotential, the total overpotential can be found adding those type of overpotential.

$$\eta = \eta_{activation} + \eta_{concentration} + \eta_{ohmic}$$

1.2.3 Activation Overpotential

Activation overpotential is the energy necessary to overcome the energy barrier of the reaction. The relation between activation overpotential and current is given by the Butler Volmer equation.

$$j = j_0 \left\{ e^{\left[\frac{\alpha_a z F \eta}{RT}\right]} - e^{\left[-\frac{\alpha_c z F \eta}{RT}\right]} \right\}$$

Where j_0 is the equilibrium exchange current and α is the transfer coefficient. The first term of the equation describes the rate of the anodic reaction, while the second term describe the rate of the cathodic reaction. The equilibrium current affects the intrinsic rate of electron transfer of the reaction. The lower the exchange current the slower the electrode reaction. The transfer coefficient indicate when the reaction is favoured at the oxidation or reduction part at a given applied potential [4]. If the activation overpotential is small, according to Taylor series of the exponential function Butler-Volmer equation can be approximate to:

$$i = \frac{i_0 n F}{RT} \eta_a$$

If the absolute activation overpotential is higher than 100mV, one of the two terms of the Butler-Volmer equation goes to zero. The equation can be rearranged as

$$\eta_a = \beta \log\left(\frac{i}{i_o}\right)$$

$$\beta = \frac{2{,}303\ R\ T}{\alpha\ z\ F}$$

The term β is the Tafel slope, which show how the overpotential changes in function of the logarithm of the current density, for Vanadium redox system z is equal to 1, R is the kinetic gas constant, T is the temperature express in Kelvin and F is the Faraday constant. In figure 1.1 is represent a graphic view of the Tafel plot.

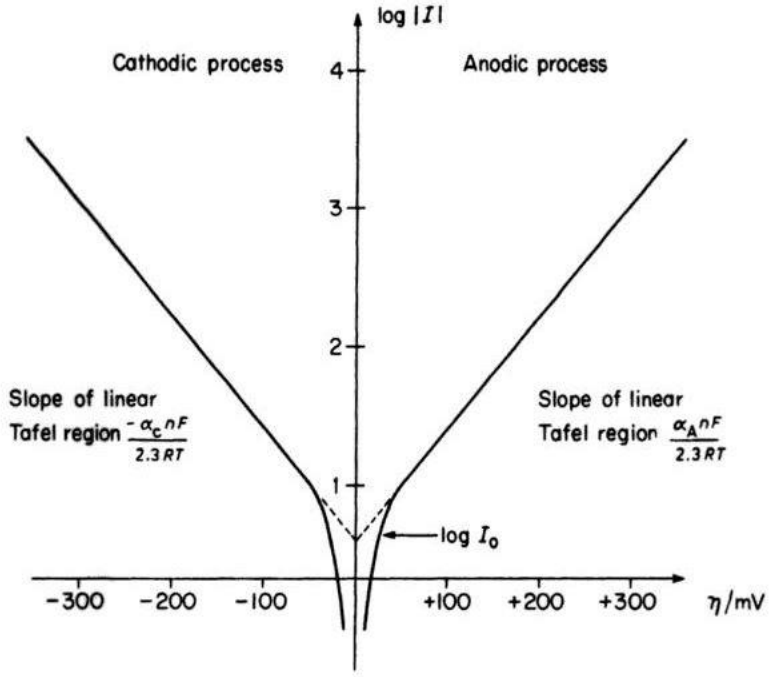

Figure 1.1: example of a Tafel plot

1.2.4 Concentration Overpotential

Concentration overpotential is given by the concentration gradient of reactant inside the electrolyte. It has a notable effect when the reaction is very fast, but the mass transport is slow: in this situation the product cannot propagate in the electrolyte and new reactant cannot reach the surface of the electrode.
The mass transport is usually carried out through:

- Migration of charged species due to the presence of an electric field
- Diffusion, from high to low concentration areas
- Convention imposed by the unbalance of force on the electrolyte, such density gradient

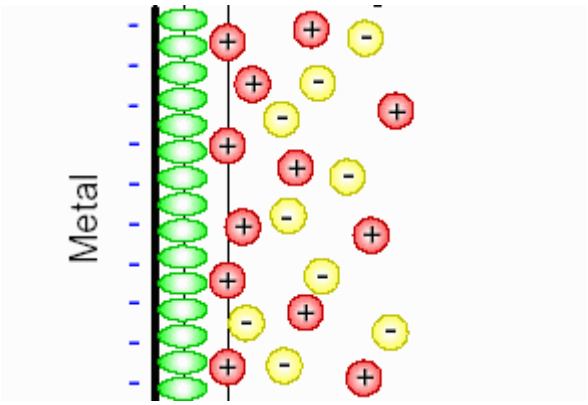

Figure 1.2: Double layer capacitance

Mass transport from the bulk electrolyte to the electrode surface is regulated by the Nernst-Planck equation

$$J_j = -D_j \nabla c_j - u_j c_j \nabla \phi + v c_j$$

First term is related to diffusion contribution, second term represent the migration and the last one is the convection term. J is the flux density of the species and D is the diffusion coefficient. When the reaction is controlled by diffusion and the electron transfer kinetic is rapid, the concentration of the reagents close to the electrode/electrolyte interface increase as the current increase with the following relation [4]:

$$i = \frac{nFD}{\delta}(c_b - c_i)$$

δ is the diffusion layer, c_i is the reagent concentration and c_b.is the bulk concentration. At specific value of current, the reagents are converted once they arrive close to the electrode surface, therefore reactant concentration tends to zero defining the limiting current at which the maximum rate of reaction is reached. The limiting current can be express as:

$$i_{lim} = \frac{nFD}{\delta} c_b$$

If the transfer by migration is negligible and the ratio between the ionic activity coefficient is assumed to unity, the generic electrode concentration overpotential can be express as:

$$\eta_c = \frac{RT}{nF} ln\left(\frac{c_i}{c_b}\right)$$

During cell operation, the concentration in bulk solution can be assumed homogeneous. A stagnant layer of electrolyte on the electrode is supposed to exist where the mass transfer is achievable only by migration and diffusion. Thickness of diffusion layer depend only on the hydrodynamic condition and viscosity of solution [5]

1.2.5 Ohmic Overpotential

Ohmic overpotential is given by the electric resistance of the cell, from the ion exchange membrane to the charge transport inside the electrolyte. The overpotential can be describe by the Ohm's Law:

$$\eta_o = iR_{tot}$$

The ohmic overpotential is linearly dependent on the applied current and the total resistance of the cell is made by the sum of electrodes, collectors, electrolyte and membrane resistance:

$$R_{tot} = R_{electrodes} + R_{collectors} + R_{electrolyte} + R_{membrane}$$

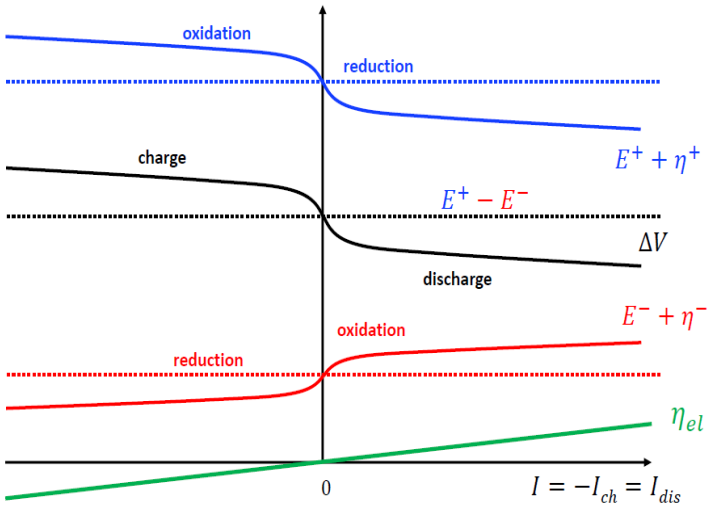

Figure 1.3: Overpotential at negative (red), positive (blue), electrolyte (green) and sum (black), different applied current

1.2.6 Theoretical Capacity

The capacity of a battery indicates how much energy can be stored as so the amount of work that the battery can afford.

The number of electrons that pass through the electrode surface is stoichiometrically correlate to the reaction development and so, for a redox flow battery, to the amount of reactant consumed and product produced. The number of electrons is measured by the total charge, Q, that pass through the circuit, can be theoretically calculate by the Faraday's law:

$$Q = xnF$$

Where x is the number of moles, n is the number of exchange electrons and F is the Faraday's constant.

1.2.7 Real Capacity

The real capacity of an EES differ from the theoretical one because the reactions at the electrodes are equilibrium reactions and so is not possible to fully complete them.

Furthermore, the real capacity is strictly correlated to the charge and discharge rate.

Increasing the discharge rate, and so the current intensity, automatically an increase of the overpotential is face. This because increasing generated current, also a higher level of

overpotential such as concentration and ohmic loss is faced, causing kinetic and mass transport problems that prevent the conclusion of the redox reaction. During a charge/discharge cycle, cut-off potential are impose to block the promotion of side-reaction such as HER in discharge or carbon corrosion and OER for the charge process as shown in figure 1.4, overpotential permit to reach those value before the effective achievement of the full theoretical capacitance.

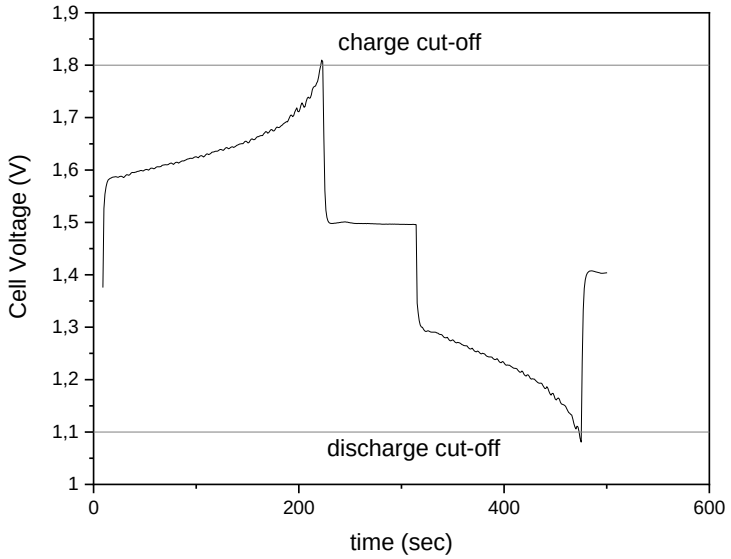

Figure 1.4: Charge/Discharge cycle and cut-off

1.3 Redox Flow Batteries

The redox flow battery architecture comes from the one of fuel cell. Generically is composed by a membrane sandwiched by two porous electrodes. The cell is connected to the two tanks, where the electrolytes are stored. Each electrolyte is pumped by an external pumping system into flow distributor of appropriate shape and geometry in order to guarantee the uniform distribution up to the surface of the corresponding electrode: the catholyte to the surface of the positive electrode, the anolyte to the surface of the negative electrode. Flow field can be of various geometry but the most used are serpentine and interdigitated as show in figure 1.6. The optimization of the distribution is a complex process because the fluid dynamic inside the cell is not trivial, this in fact depend on electrode's porosity, thickness, electrolyte viscosity and temperature.

The ionic exchange membrane divides the two-semi cell and permit the proton flux passage for the energy balance, denying passage of electrons and short circuit. On the electrode, placed in contact with the current collector reaction occur on the active sites.

The redox couple defines the equilibrium potential of the cell, thus determining the cell voltage. Redox couples can be divided into inorganic and organic. Inorganic ones are often metallic ions; they are more expensive but better performing and immune from capacity-fading phenomena. As a result, they are much more durable than organic ones, which are cheaper but suffer from faster degradation as they tend to undergo side reactions when oxidized or reduced.

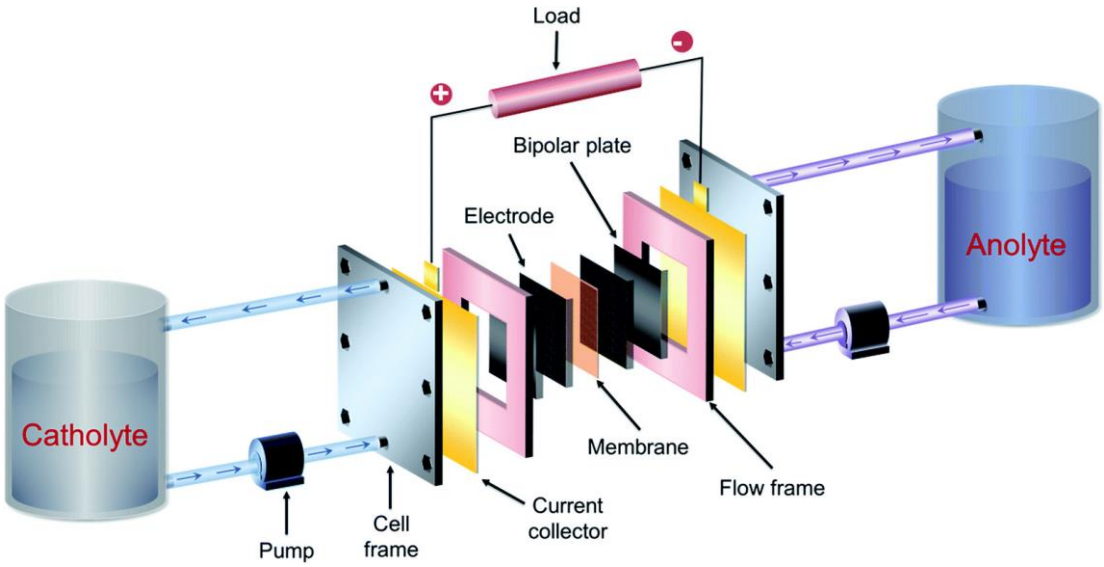

Figure 1.5: Cell architecture of a RFB

At an industrial scale, gas diffusion layers (GDL) are used as electrodes for VRFBs. GDLs consist in a network of graphitic carbon fibers, usually made from electrospinning and pyrolysis of polyacrylonitrile (PAN) precursors [6]. The most common electrodes that could be find are carbon felt, carbon paper and carbon cloth.

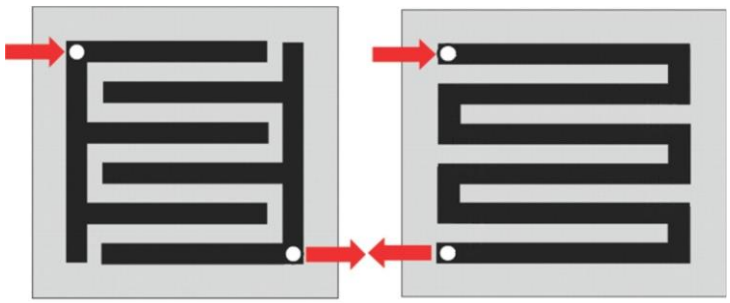

Figure 1.6: Different flow field distributor, interdigitated left, serpentine right

Together, redox couple and electrolyte are also responsible for the density and viscosity of the solution, which in turn have an effect on the whole fluid dynamics of the system, including the required pumping power, convection and diffusion of the electrolyte through the electrode surface. The most promising couple of ions is the one made by the different oxidation state of Vanadium on both the semi cell.

1.3.1 Vanadium Redox Flow Battery

Vanadium has the peculiarity to have four oxidation state, the usage of this ion on the redox flow battery permit the possibility to recover and restore the electrolyte even after cross-over contamination. Cross-over contamination happen when the electrolyte of a semi cell, pass by diffusion through the protonic membrane to the other semi cell, this led to a lowering of the maximum capacity of the battery influencing so the efficiency.

At anode, the couple V^{2+}/V^{3+} and at the cathode the couple VO^{+2}/VO_2^{+}, namely V^{4+}/V^{5+}.

The reaction can be list as follow:

anodic reaction: $V^{2+} \leftrightarrow V^{3+} + e^{-} \qquad E_0 = -0{,}26V$

cathodic reaction: $VO_2^{+} + 2H^{+} + e^{-} \leftrightarrow VO^{2+} + H_2O \qquad E_0 = +1{,}004V$

The combination of anode and cathode reaction bring to a theoretical cell potential of 1,259V. On the electrodes, other type of reaction may take place, those reaction are parasitic reaction and could degrade the electrodes. The most dangerous reaction are the hydrogen

evolution, oxygen evolution and carbon corrosion that occur at the anode and cathode, respectively.

$$2H^+ + 2e^- \leftrightarrow H_2 \qquad (0\ V)$$

$$2H_2O \leftrightarrow O_2 + 4e^- + 4H^+ \qquad (1{,}23\ V)$$

The potential reaction is measured in respect to the one of HER.

1.3.2 State Of Charge

The state of charge of a cell indicate the level of energy stored inside the battery and so the capability of load a circuit, SOC goes from 100% to 0%. In a Vanadium Redox Flow Battery (VRFB), the value of SOC depend on the volume of the electrolyte tanks and is function of the Vanadium concentration responsible of the discharge reaction. Since in VRFB are present two tanks for the two electrolytes the SOC can be calculated for both semi cell. SOC calculated for the negative side take the name of negative SOC and positive SOC for the one calculates on the positive side of the cell, the lowest value of SOC is the practical SOC of the cell. If the volume of the two tank is equal, the SOC can be calculated as follow:

$$SOC = \frac{[V^{2+}]}{[V^{2+}] + [V^{3+}]} = \frac{[V^{5+}]}{[V^{5+}] + [V^{4+}]}$$

This relation is valid just if cross-contamination is not considering and if the concentration of the two solution remain constant in time (no degradation process). An alternative form of SOC equation, in a more general way can be:

$$SOC = \frac{[V^{2+}] + [V^{5+}]}{[Vtot]}$$

State of charge value can be evaluated by measurement of open circuit potential by usage of this equation, derived from Nernst equation:

$$E_{cell} = E_0 - \frac{RT}{nF}\ln\left(\frac{[V^{3+}][V^{4+}]}{[V^{2+}][V^{5+}][H^+]^2}\right) = E_{0cell} - \frac{RT}{nF}\ln\left(\frac{(1-SOC)^2}{SOC^2[H^+]^2}\right)$$

The real correlation between SOC and OCP is valid only in the linear range of the polarization curve as show in the figure 1.7

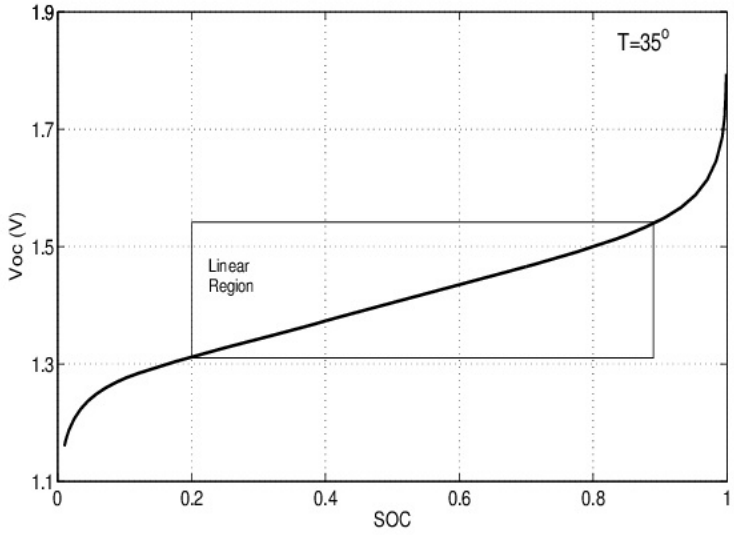

Figure 1.7 : OCV at different SOC

1.4 State Of Art

The commercial VRFB available on the market are made by industrial component from fuel cells as the Nafion membrane and the electrodes that are used as gas diffusion layer (GDL) on fuel cells. A detailed explanation of the VRFB component is discuss in the next section.

1.4.1 Electrodes

Electrodes for VRFB need to have some characteristic in order to increase the efficiency:

- High electric conductivity
- Catalytic activity toward the reactions
- High superficial area, so to increase the surface available for the reaction

- Chemical and mechanical stability: since those electrodes are immerse in acid solution and undergoes mechanical flexion by the flux of electrolyte, they must resist to chemical and mechanical degradation.
- Selective permeability: electrodes morphology must be suitable for the diffusion of the solution

GDL's has a good trade-off of the request for good electrode. High electric conductivity permits the fabrication of this electrodes by fibers, so to increase the superficial area and porosity. GDL's can be of three type: paper, cloth and felt, microscope image of those three different types of GDL are shown in figure 1.8.

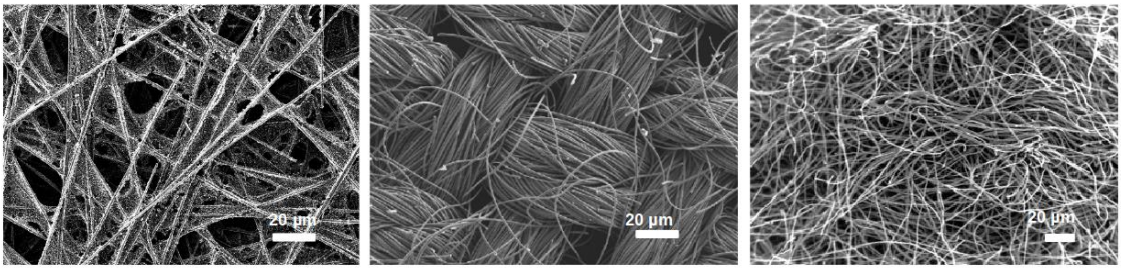

Figure 1.8: Sem view of different GDL type: carbon paper, carbon cloths and carbon felt

Any of this morphology give a different fluid dynamic and a different electric conductivity. Is important to match the electrode and the flow field in order to increase the mass transport and the reaction kinetics. A detailed analysis of the carbon in GDL show that is made of sp^2 carbon [7] [8], each fiber is compose by more graphite layers, the edge of any plane is responsible of the catalytic activity toward the reaction of redox of Vanadium [9] [10].On figure 1.9 summarized the three-step mechanism proposed by Wei *et al.* [6]

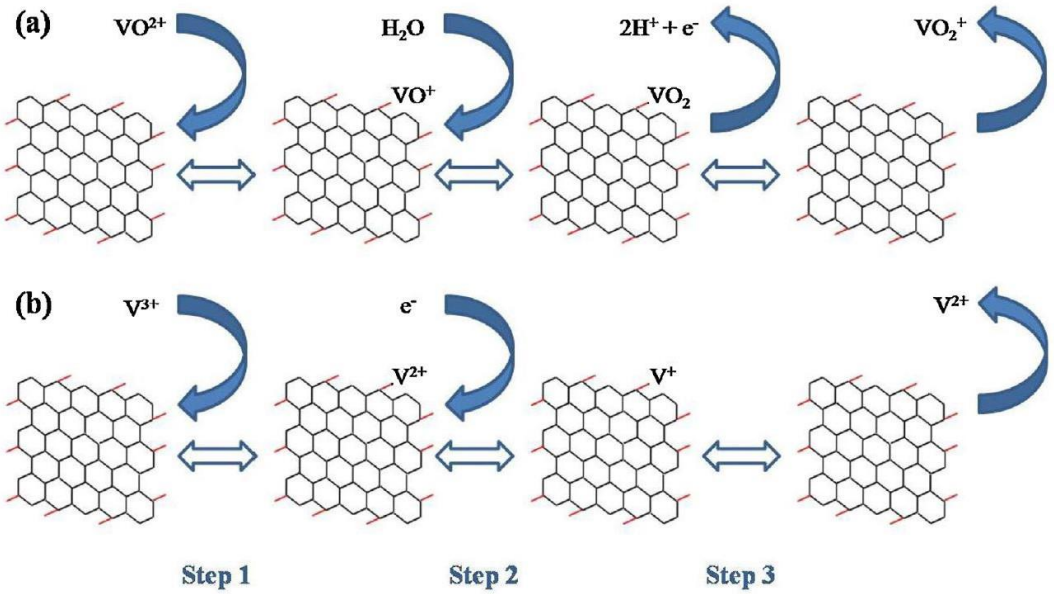

Figure 1.9: Scheme of the reaction mechanism of Vanadium at graphite edge plane

Despite the good trade, vanadium redox flow battery suffers still a sluggish kinetic, on the negative side relevantly. To increase the kinetic, is possible to work in two direction: increasing the catalytic activity or increasing the number of active sites for the reaction.

For the catalytic activity, the increment is possible by insertion of functional group on the graphite structure backbone, that functionalization could be reach by thermal, chemical or electrochemical treatment.

Introduction of Oxygen on the edge of graphite, is effective in boost the kinetics, such as the introduction of Sulphur, Phosphate, Zirconia and metallic particle of Bi and Cu [11] [12] [13], because the d and p orbitals could attract in an efficient way Vanadium ions and help on the adsorption of those species for the coordination of reaction. The other method for enhanced efficiency is proposed by Zhao *et al*. An etching method with KOH is been propose in order to increase the superficial area [14] [15]. By this technique is possible obtain two type of pores (in addition to the one of the GDL), micropores and nanopores, the first are responsible of an efficient permeability of the solution through the electrode, the latter, increase notably the surface area and active sites.

Another technique to increase the surface area is to cover the carbon fibers with a material with higher porosity. This goal is reachable by immersion of the electrode in a nanoparticle colloidal suspension and drying the coated electrode [16]. A new method is to deposit onto the graphite fiber a material with a higher surface area than the graphite itself. This latter

method is the one adopted in this thesis for the fabrication of a new electrode suitable for vanadium redox reaction. Major details are given at chapter 2.

1.4.2 Membrane

The membrane in VRFB split the battery in two semi cells, making a bridge between anolyte and catholyte, permitting the protonic exchange and disabling the diffusion of ion responsible of SOC's battery. For those materials, a high protonic conductivity and low electronic conductivity are required. The membrane conductivity depends on the humidity, since the positive charge are drag by ions as hydronium and water molecules, the humidity is so a fundamental parameter for a good work of the membrane. Furthermore, the membrane must resist on highly acid solution and have good mechanical properties. Nafion membrane is the most used membrane for this application but various type of membrane could be suitable for VRFB, the IEM (ion exchange membrane) can be further divided in heterogeneous and homogeneous, the other class is non-ionic porous membrane (PM). Factors as morphology, selective permeability, mechanical properties and swelling can be tuned by the production method [17].

1.5 Losses and Degradation Mechanisms of VRFB

In order to understand and quantify the performance of VRFBs, it is useful to define some quantities commonly adopted to evaluate batteries efficiency. Coulombic efficiency (or faradaic efficiency) describes the charge efficiency by which electrons are transferred in a system involving an electrochemical reaction. In a battery, it is defined as ratio of the total charge extracted from the battery to the total charge put into the battery over a full cycle.

$$\eta_c = \frac{C_{discharge}}{C_{charge}} = \frac{I\ x\ \Delta t_{discharge}}{I\ x\ \Delta t_{charge}} = \frac{\Delta t_{discharge}}{\Delta t_{charge}}$$

Voltaic efficiency is instead defined as the ratio of average discharge voltage to the average charge voltage.

$$\eta_V = \frac{V_{discharge}}{V_{charge}}$$

While coulombic efficiency account for all losses that might take place in a charge-discharge cycle of a battery, voltaic efficiency is very useful to isolate mass transport and redox kinetics. However, the overall behavior of a battery performance is better described by the energy efficiency, which is simply the product of coulombic and voltaic efficiency. It represent the ratio between the energy released in the discharge phase and the energy needed for the charge phase [18] [19]. Many phenomena can prevent from obtaining good efficiency, since the VRFB system contains several key components, each having its own limits and degradation mechanism.

1.5.1 Electrolytes Degradation

The main issue concerning the electrolyte is the solubility limit: in fact, the solubility of each ion is a function of temperature, sulfuric acid concentration and SOC. At elevated temperatures (above 40 °C) V_2O_5 tends to precipitate, possibly causing blockages in the stacks and in the pumps. On the contrary, VSO_4, $V_2(SO_4)_3$ and $VOSO_4$ suffer from poor solubility at low temperatures. Thus, the maximum vanadium ions concentration is 2M, which results in a maximum energy density of 25Wh/kg. The operating temperature range is limited to 10 °C to 40 °C [20] [21].

In order to mitigate those effects, alternative electrolytes have been proposed, like a mixture of hydrochloric and sulfuric acid that raised to 2.5M the solubility limit of vanadium ions [22]. Long-term stability, however, is still to be investigated. A more common solution consists in the use of additives and precipitation inhibitors, both organic and inorganic. Ammonium phosphate, for example, can extend cell operation for a 2M vanadium solution without precipitation. Also, K_2SO_4, $(NaPO_3)_6$ and CH_4N_2O can inhibit V^{IV} precipitation in a 4M super-saturated solution. Again, these results are still under investigation, especially regarding stability issues and effective use in both the anolyte and the catholyte at the same time [23] [24]. In addition, the anolyte solution needs some extra care, as it suffers from oxidation of the V2+ ion in air. The reaction happens with a high rate at the electrolyte/air interface, which must be minimized. V^{2+} oxidation reduces the available charge, influencing energy capacity of the system [24].

1.5.2 Electrodes Degradation

A key component that is subject to degradation phenomena is the electrode. The focus will be on carbon-based electrodes since they are the standard for VRFBs. A combination of many different factors is likely to be responsible for electrode degradation, including

thermal, mechanical, chemical and electrochemical effects. The latter is the most recognized form of damage, and most relevant to this work.

Electrochemical degradation of carbon electrodes is commonly referred as carbon corrosion, and it also constitutes one of the side reactions that can occur in a vanadium flow battery. The standard potential for carbon corrosion is 0.207V vs SHE, but the reaction rate becomes relevant only at higher potentials, when the local SOC in the solution is around 100% and the competitive vanadium ions oxidation is not present anymore [25]. In the positive half-cell, carbon corrosion resulting in CO and CO2 evolution can take place (with a relevant rate) at 1.35V or higher, according to the following reactions:

$$\mathrm{C} + \mathrm{H_2O} \rightarrow \mathrm{CO} + 2H^+ + 2e^-$$
$$\mathrm{C} + 2\mathrm{H_2O} \rightarrow \mathrm{CO_2} + 4H^+ + 4e^-$$
$$\mathrm{C} + \mathrm{H_2O} \rightarrow \mathrm{CO_2} + 2H^+ + 2e^-$$

These reactions not only affect the electrode activity due to loss of surface area and change in surface functional groups, but they are also responsible for a current consumption that lowers energy efficiency of the system. Also, the formation of bubbles due to gaseous products disturbs the mass transport of reactants to the surface of the electrodes [26]. However, carbon corrosion is expected to take place at a significant rate only at high temperature and in presence of catalysts.

1.6 Cost and existing VRFB

Even if VRFB is one of the most promising technology for the energy storage of grid levelling, their displacement is brake from the high realization cost, the low power and energy density. The battery cost in general depend on the set-up of the application, that's because stationary cost and variable costs are present. The set-up of an VRFB ESS depend on various factors: cell voltage, current density, vanadium concentration and material costs. Is so evident how the price is correlated to the technology aspect. Zhao [27], ming-jia [28] proposed a methodology for the cost and profit calculation derivable from the installation of a VRFB for stationary use.

In the example reported in [29] the cost for a Vanadium Redox flow battery energy storage system of 20MW, 160MWh with a depth of discharge (DOD) of 0,6 is calculated. The calculation is based on assumed voltage and coulombic efficiencies of 80% and 99%,

respectively. The resulting energy efficiency is 79%. The target function is a simple linear cost function describing the overall system costs C_{system} as sum of costs of power and energy subsystems, with a cost rate of power subsystem C_{power} and a cost rate of energy subsystem C_{energy} calculated on the basis of the technical configuration. Cost associated with the installation are several: among them operation and maintenance (OM) cost, both fixed and variable, power connection system (PCS) and balance of plant (BOP) [30].

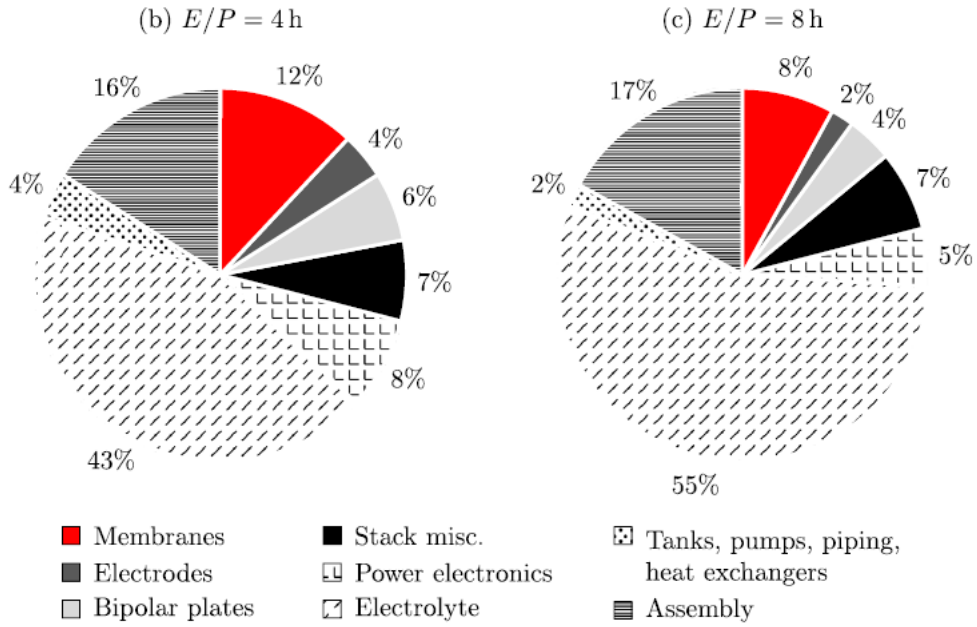

Figure 1.10: Percentage of different costs contribution on 20MW VRFB plant, (b) 4 hours discharge and (c) 8 hours discharge [29]

As is visible for figure 1.10 Vanadium plant costs depend on the total amount of energy request and on the time for discharge. For a higher time for discharge a larger electrolyte tank and volume is request, increasing the relative cost of the energy subsystem. The operation point determined from the electrochemical is defined by a current density i=1 kA/m^2 and a cell voltage in charge and discharge mode of U_{charge} =1,555 V and U= 1,244 V, respectively. Corresponding cell powers are $P_{cell,charge}$ = 4,241 kW and P_{cell} = 3,360 kW, with a cell area of 2,7m^2. On the C_{power} are included the costs for the electrochemical cell, system control costs and stack assembly costs. C_{energy} costs depend, of course, on the tank capability, electrolyte volume, concentration of vanadium, pumps and heat exchanger. PCS costs are proportional to the power system, while cost correlated to the electrolyte, tank etc. are proportional to the capacity of the system.

Material assumption for the assessment are carbon felt as electrode, Nafion 117 membrane, polyethylene gasket, graphite bipolar plate and copper current collector. This studies result shows a simple linear function for system cost.

$$C_{system} = P \cdot C_{power} + E \cdot C_{energy}$$

The cost structure of a stack is dominated by the membrane (37%). Carbon felt electrodes and BPP account for 11% and 19%, respectively. Further stack components have a share of 21%, while stack assembly accounts for 12% of total costs. Electrolyte costs account for about half the system costs (43%; 55%). Despite for a large displacement of this technology a further innovation is required, on the last years several plants have been installed both for high and low accumulation capability system.

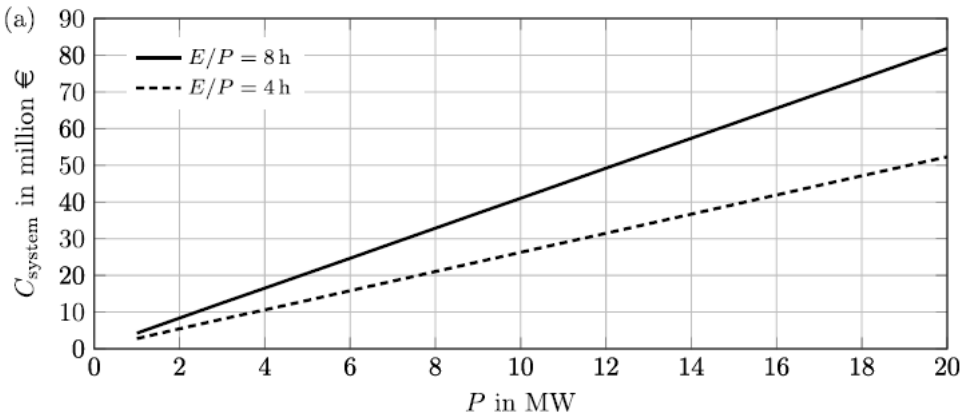

Figure 1.11: Linear function of cost related to plant power [29]

In figure 1.11 is shown the linear function of cost system related to plant power, for an plant power of 20MW and 8 hours of discharge time (160MWh), a total system cost of 81,9 Million € is needed.

One of the first appliance, based on the University of New South Wales license Thai Gypsum Products installed 5 kW-12 kWh VRFB to support a 1 kW photovoltaic (PV) power system in Thailand. The battery was designed to store solar energy during the day so it could be used at night. On the website of the energy department of united states is possible to have a list of al the project financed, in construction and announced all over the world.

Here are reported some of them, only the project with a power higher than 600KW.

Title	**Country**	**State**	**Power KW**	**Capacity (hours)**
ilton-IESO	Ontario	Contracted	2000	4
Minami Hayakita Substation Hokkaido Electric Power- Sumitomo	Hokkaido	Operational	15000	4
V.C. Bird International Airport of Antigua Solar/Energy Storage Project - PV Energy Ltd	Antigua and Barbuda	Operational	3000	4
The Zhangbei Project - State Grid / Sparton Resources	Hebei Province	Operational	2000	4
Ontario IESO - SunEdison / Imergy Flow Battery	Ontario	Contracted	5000	4
Guodian Hefeng Beizhen Wind Farm: VFB	Liaoning	Operational	2000	2
Guodian Longyuan Wind Farm VFB - Rongke Power & Anshan Rongxin	Liaoning	Operational	5000	2
Washington State University 1 MW UET Flow Battery - Avista Utilities	Washington	Operational	1000	3,2
Tomamae Wind Farm	Hokkaido	Operational	4000	1,5
Yokohama Works Energy Storage System - Sumitomo Electric Industries, Ltd.	Kanagawa	Operational	1000	5

Table 1.1: VRFB system for stationary energy storage [19]

1.6.1 Domestic VRFB

Even if the main focus of the VRFB technology is the storage of energy from smart grid and deployment of energy for large scale, another interesting utilization of this technology is for domestic energy storage. The dominant technology used for this scope is the lithium ion battery, that with its efficiency and standardized process offer an high efficiency, low costa energy storage system, the problem of LiB fall in the low life cycles, and impossibility of decouple power and energy system.

Despite their low current density and power density, Vanadium Redox Flow Batteries are starting to be introduced into the market, in fact, a Dutch Start-up named VoltStorage, has made the first vanadium flow battery energy storage system for domestic application, in order to store the energy provided by a photovoltaic system and deploy electricity during the night or in not-suitable weather condition. The star-up has received investment of 110m € from Softbank [31] and private investor, showing an effective interest from the financial word in this technology and in the development of a possible alternative to LiB.

1.7 Purpose of this work

This work was conceived with the prospective to explore a new way to obtain electrodes for VRFB with a high surface area. By increasing surface area is possible not only to obtain more energy and power density, but also to decrease the geometry and the stack dimension and so the relative costs of plant that are the 45% of the total. Furthermore, the cell geometry enhances the overpotential. By decreasing the overpotential it will be possible to reach higher current, without promote parasitic reaction as HER or OER. Surface is so one of the most important parameters to control, in order to open the possibility to use those battery in the energetic storage system of grid levelling and to deploy it on the smart grid. At the Istituto Italiano di Tecnologia (IIT), objective in this direction are already been undertake, by using a novel technique of non-thermal plasma deposition, carbon based electrode and nitrogen-carbon electrode, both with high surface area have been developed [32] [33].

The synthesis is carried out with a prototypal PECVD deposition source, which allows high deposition rate on large area starting from gaseous precursors. The aim is to correlate electrochemical performance to material properties, in order to evaluate what are the main features that determine a good efficiency and surface area. The synthesis is performed by a novel instrument made in IIT, the NanoJeD. the instrument underwent some improvement

by increasing the vacuum power, numerous tests have been needed for the calibration of the instrument in order to continue to deposit the same materials my co-worker made.

Starting from the procedure already established by predecessors, this work expands the thermal treatment to higher temperature, in order to increase the graphitization and so the conductivity and electrocatalytic activity, formation of carbon allotropes are expected during thermal treatment. Study of electrochemical properties are made depositing the material on glassy carbon (GC) and test in an electrochemical cell at three electrodes, in a solution on 2M sulfuric acid where 0,1M vanadium ions are dissolved. The SOC of the electrolyte is 0%. The best samples are then deposited on GDL and tested in a symmetric and full cell at the MRT POLIMI Lab. Finally, the impact of this new nanostructured carbon electrodes on the over all economics of a vanadium redox flow battery system is evaluated.

Chapter 2
Deposition Parameter

2.1 NanoJeD System

NanoJeD is a PECVD where the nanocrystal formation zone is split from the collection chamber by a thin slit. The vacuum pump is place at the bottom of the system while the gas precursor is introduced from the top, the structure of the NanoJeD follow a vertical development where the gas pass through some stages of formation of the nanocrystal and collection of the substrate. The slit is thin enough to produce a supersonic jet, leaving the chambers at two different pressure. On figure 2.1 is possible to see a schematic view of the NanoJeD.

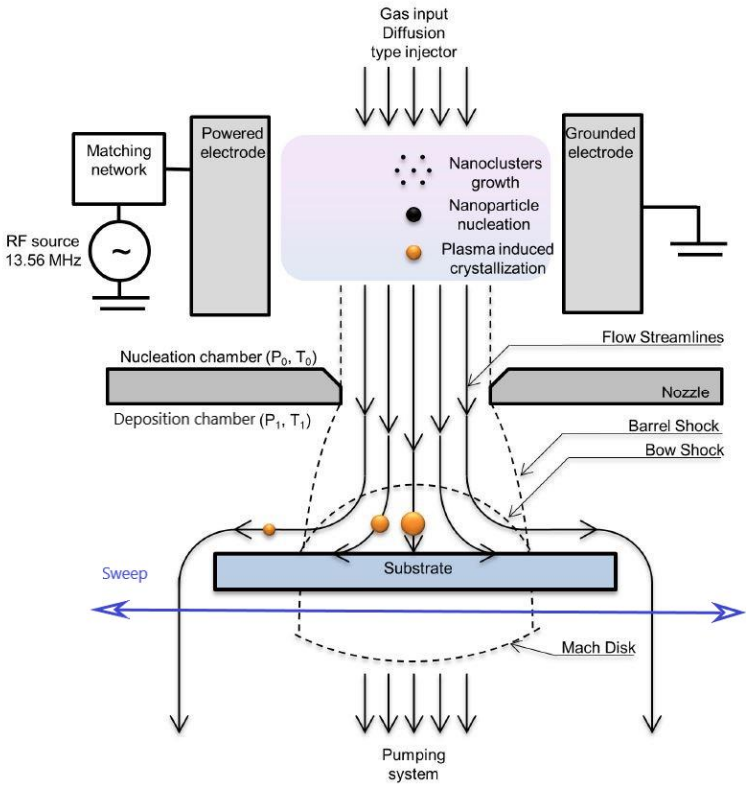

Figure 2.1: scheme of NanoJeD system [34]

In the upper chamber (reaction chamber) a gas precursor is injected in between two electrodes: the anode is grounded, and the cathode is fed with a radio frequency (RF) signal, conveniently tuned in its phase and amplitude with a matching box. The RF signal ignites a low pressure non-thermal plasma: precursor molecules owing between the electrodes are dissociated into radicals that start to polymerize in few-atoms, clusters and then into nanoparticles. Precursor could be any gaseous mix, as demonstrated in other work with the same source where silane was used to produce silicon [34].

The synthesized particles are then collected in the supersonic jet and accelerated in the lower chamber (impact chamber). The impaction of NP happens at room temperature, so any substrate can be employed. Just below the orifice, the sample holder is swept back and forth by a movement system, allowing to have deposition on a wider area.

The peculiarity of the source is that the supersonic jet decouples the two chambers, and permits to independently control NP and film properties, since plasma parameters tune crystallinity, chemistry and particle size while impaction chamber pressure allow to control particle packing. The source deposition area is limited simply by geometrical constrain

because depend on slit width, giving the source an easy scalability and making it compatible with roll to roll, large scale production systems.

2.2 Upper Chamber

2.2.1 Non-Thermal Plasma Nanocluster And Nanoparticle Synthesis

Plasma is considered as the fourth state of matter: basically, it is a quasi-neutral ionized gas containing freely and randomly moving electrons and ions. Plasma's theoretical aspects are not described in detail because out the scope of the work. For a more in-depth discussion on plasma theory references are made to specialized books [35] [36].

In the non-thermal low energy generated plasma, the presence of a strong oscillating electric field in the region close to RF powered electrode's surface cause the breakdown of atoms/molecules into electrons and ions and the acceleration of mainly electrons, due to their lower mass with respect to ions. The electrons have a main energy of 2-5 eV while the ion and neutral species have a lower main energy of about 25 meV. The collision between high energy electrons and neutral species lead to the formation of radical atom that start the nucleation by reacting from each other promoting formation of nanocluster.

Gas residence time is a crucial parameter because controls few-atoms cluster agglomeration, that is a concentration and time-controlled process [37] [38]: it also determines, together with plasma reactions, nano-particles growth and final size and can be tuned working with fluid-dynamic parameters. The residence time of a single particle in the reaction zone controls the size distribution dispersion: in the NanoJeD source the flow in the upper chamber is laminar and the streamlines are parallel to each other's, matching gas and particle residence time.

2.3 Lower Chamber

2.3.1 Nanojed Fluidodynamics

Fluid dynamics inside the NanoJeD system is not trivial. the difficulty comes from the differences in flux regime and so the many different Knudsen number: in the upper chamber, the gas is on a laminar regime (Kn lower that one), while in the supersonic jet the regime the

impact between molecules are null and so the Knudsen number is much higher than one. Passing from Kn minor than one to major one, a transient regime is established in the slit.

The dusty-gas is then forced to flow through the orifice, accelerating up to speed of sound in the slit's throat and expanding in the lower chamber: gas expansion proceeds until a certain distance from the orifice, called Mach disk, where the gas recompresses. For an arbitrary upper chamber pressure and slit geometry, the gas flux through the slit is given by the chocked flow condition, caused by the supersonic jet. The gas speed in the orifice is the speed of sound *a*, and it depends on gas type (and molar mass M) and temperature:

$$a = \sqrt{\frac{\gamma T R}{M}}$$

The definition of speed of sound allow to also define the Mach number:

$$M = \frac{v_{gas}}{a}$$

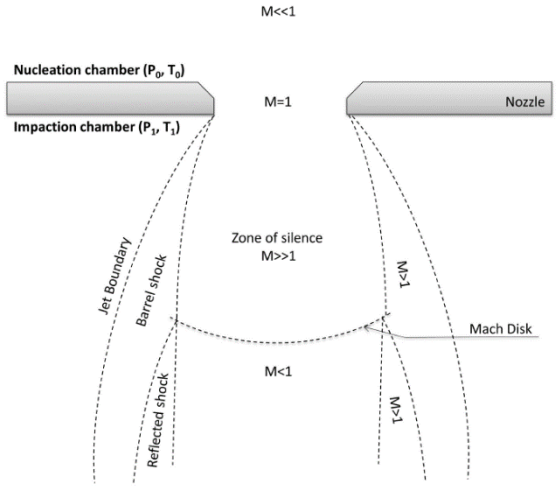

Figure 2.2: scheme of different Mach zone in the lower chamber

Without a convergent-divergent nozzle, is not possible to achieve in the orifice's throat Mach number higher than one.

Once the slit orifice is pass, the gas undergoes expansion cooling thus the temperature and promoting a quenching of the nanoparticles [39]. Figure 2.2 show the different zone under the slit and the relative Mach number. Detailed study of the dynamic under the orifice is out of this work's purpose.

Once the particles are in the impact chamber, they are decoupled from the gas stream and their path is define by their own inertia. The decoupling of particles and gas stream is the key for a controlled collection of the NPs on the substrate. The value of the inertia ratio between particle and gas stream, defined Stock's numbers (St) that quantifies the balance between the inertial and the fluid forces acting on the single nanoparticle moving in the jet stream. When the former is dominating (St > 1) the particle is impacted on the substrate, whereas in the opposite case (St < 1) it follows the gas streamlines escaping collection.

$$St = \frac{Particle\ Inertia}{Fluid\ Forces} \propto \frac{Particle\ diameter}{Pressure\ lower\ chamber}$$

Particle inertia is strongly correlated to their kinetic energy, placing the substrate closer to the orifice, collection of smallest particles is possible, film's morphology will be dense uniform and compact. In the opposite way, distancing the substrate to the orifice, only accumulation of higher particle, with higher kinetic energy and inertia is possible, leading to the formation of a porous hierarchical assembled film.

Gas expansion in limited to the barrel shock and end in a stationary wave called Mach Disk, place at a distance Xm from the orifice [40], as show in figure 2.3

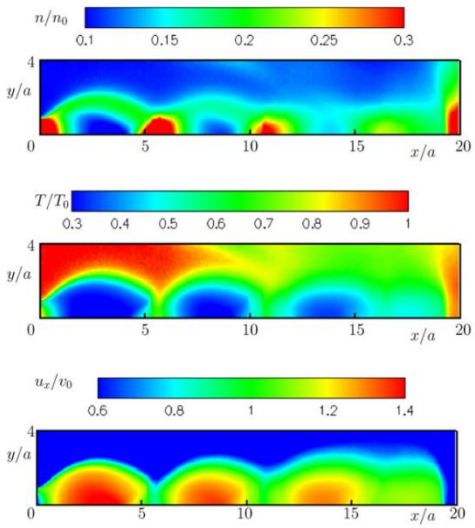

Figure 2.3: position of Mach disk [40]

At lower value of X_M, the gas recompressed, until reaching the same pressure value of the impact chamber, decreasing velocity and so the Mach number. X_M value is important to define the impact energy of the particles during the deposition. X_M depend on orifice geometry and ratio of the pressure in the two chambers, expression of X_M is show in equation 2.4

$$X_M(mm) = 0{,}67 \sqrt{\frac{P_0}{P_1}} \left(\frac{l}{w}\right)^{0{,}47} w$$

This expression holds for Kn << 1 and R >> 10, that mean in viscous regime.

The holder's distance to the orifice is define as X. The ration between X and X_M, called **Ω** (**Ω**=X/X_M) the impact energy and so the collection method of the nanoparticles. This is another fundamental parameter in NanoJeD, because is one of the responsible parameters to tune the morphology. Is possible to define two limit cases:

- **Ω** << 1: high kinetic energy monodirectional impaction.In this first scenario, the substrate is placed inside of the supersonic expansion, forcing the gas streamlines to be deflected at the substrate location and to form a recompression wave, the Bow Shock. The nanoparticles are accelerated at high speed in the supersonic jet (for a nanoparticle diameter of 5 nm the

average kinetic energy is in the order of 0.1 - 0.2 eV atom-1) and they experience virtually no collisions with the background gas molecules. The resulting film is characterized by a dense morphology (maximum theoretical density for a dense aggregate of close-packed spheres is 50 - 64%).

- $\Omega >> 1$: soft landing with randomized landing direction. In this second condition the substrate is located below Xm. The average speed of the particles is lowered, and the recompression wave force the nanoparticles to scatter among themselves and with the gas molecules, causing self-assembling in the gas phase and randomization of their landing direction. The resulting film is characterized by a porous morphology and, in a certain window of the processing parameters, the formation of quasi 1D hierarchical tree-like nanostructures can be obtained.

For fixed X, the value of the Ω parameter can be finely adjusted by changing P_1.

2.4 Thermal Treatment: Annealing

Despite the attempt to obtain a crystalline material by employing high RF power in the deposition process, as-deposited films are expected to be amorphous, hydrogenated and thus poorly conductive. This is confirmed by Raman (Chapter 3.1).

To get a material that suits the established requirements, it is necessary to remove hydrogen and increase crystallinity (which corresponds to graphitization degree for carbon nanoparticles). Temperature can increase the graphitization degree of as deposited nanoparticles and induce more defects on the graphitic planes, so an annealing procedure is necessary [41].

An annealing procedure at high temperature, ultra-high vacuum in a controlled atmosphere allows to obtain graphitic, hydrogen-free, conductive films. As-deposited films have been annealed in vacuum (P 10^{-3} Pa), with a dwelling time of 2 hours. Different temperatures have been tested, in order to find an optimum. Chosen temperatures are: 800 °C, 900 °C, 1000 °C and 1100 °C. Annealed samples have been characterized and tested.

2.5 NanoJeD Settings

Many operational parameters can be regulated while using NanoJeD, each with different results on the final material properties. With the aim of synthesizing films with the characteristics of a dense, compact and uniform coating, the choice of deposition settings is

described in this section. All depositions have been carried out on silicon and glassy carbon substrates, the former being more suitable for morphological characterization while the latter is needed as an electrically conductive support for electrochemical testing.

The parameters of interest are:

- Gas composition: gas mixtures made of an inert gas and a reactive species are used for the deposition of nanoparticles with NanoJeD. Besides giving the material composition, precursor gas dilution will determine particles size: increasing the amount of reactive gas in the mixture, larger nanoparticles are obtained. In this work, a acetylene-argon mixture is used in the following proportion: C_2H_2= 1,6% Ar=98,4%. This small dilution is chosen to keep nanoparticles size small.
- Gas pressure: In this work, gas pressure is kept constant at 130Pa, this value is chosen to keep a ratio pressure over the two chambers higher than hundred, this value is so limited by the power of the vacuum system.
- RF power: RF power affects the degree of precursor dissociation in plasma, giving different mass deposition rates. In order to achieve a high deposition rate and maximize particles crystallinity, the maximum obtainable RF power has been used, in this case equal to 120W.
- Geometrical factors: electrodes distance influences plasma density (i.e. electrons concentration per unit volume). Here, it is arbitrarily set to 50mm. Slit width determines the conductance, defined as the ratio between throughput (Q) and pressure drop across the orifice (ΔP)

$$C = \frac{Q}{\Delta P}$$

Conductance affects compression ratio and thus impact energy of the particles and film density. A lower bound on slit width is given by RF matching, which becomes unstable below a certain width; this happens at 1mm, which has been chosen for this work in order to maximize the pressure drop. Slit length, together with the sweep amplitude, directly gives the total deposition area.

Chapter 3
Material Characterization

3.1 Raman Characterization

Raman spectroscopy is a technique used to study vibrational modes, exploiting inelastic scattering of monochromatic light. Raman spectroscopy is used for the investigation of the carbon structure in terms of hybridization and disorder and to understand how are correlated with synthesis process parameter. When a sample is illuminated with a monochromatic laser beam (typically in the visible range), most of the radiation is either absorbed, transmitted, reflected or elastically scattered (Rayleigh scattering). However, a small portion of the incident radiation suffers from inelastic scattering, generating Stokes and antiStokes photons, which are re-emitted (from a virtual energy state) at a lower and higher frequency with respect to the incident photons, respectively. This change in frequency comes from the inelastic scattering process between photons and vibrational modes in a crystal (phonons). Stokes and anti-Stokes photons are collected, and their frequency gives information about the chemical composition and bond types of the sample. A vibrational mode is Raman-active only if the vibration induces a change in the polarizability (α) of the molecule/crystal. For crystals there are some selection rules that result in the possibility to detect only optical phonons close to the center of the first Brillouin Zone.

Raman spectroscopy is sensitive to the structural order of a crystal. For this reason, it can help in gathering information about the microstructure of the studied samples, not only about their chemical composition. A perfectly crystalline material, in fact, shows sharp peaks in the Raman spectrum. Spectra of nanocrystalline and amorphous materials, on the contrary, are characterized by broadened and shifted peaks, because of a relaxation of the selection rules. Thus, more vibrational modes, far from the center of the first Brillouin zone, are involved. All the Raman measurements done in this work have been done using 532 nm wavelength.

3.1.1 Raman Spectroscopy Of Carbon Structure

The case of carbon-based materials is quite peculiar and it has been studied extensively [42] [43] [44]. Each allotrope (i.e. diamond, graphite) has its own peaks and the level of structural disorder affects their width, position and relative intensity. Graphite characteristic peak is the G peak (1580 cm^{-1}), which is attributed to the E2g vibrational mode. Its physical origin resides in the in-plane stretching mode of C – C sp2 bonds belonging to both chains and rings. In the case of not perfectly crystalline graphite, another peak arises, called D peak (1350 cm^{-1}); it is attributed to the A1g breathing mode of carbon rings. This signal is visible only in non-perfectly crystalline graphite, and its intensity increases as the size of the crystalline domain decreases, up to the limit of a completely amorphous carbon (e.g. glassy carbon), where the size of the crystalline domain is zero.

To follow a quantitative approach, spectra need to be fitted in order to obtain precise information and to extrapolate information on hybridization and defectiveness, that will determine conductivity and activity towards vanadium ions. The fitting of 532nm Raman spectrum for carbon material is widely used and in literature are proposed several approaches, each one depending on the type of carbon of subject. For graphitic carbon, the recommended fitting procedure consist in the use of a Lorentzian distribution for D peak and a Breit-Wigner-Fano (BWF) for G peak. For amorphous hydrogenated carbon, the case of as deposited sample, different approaches can be employed, for example four Gaussian fitting and a baseline, or alternatively two Gaussian, a Lorentzian for D, a BWF for G and a baseline. For carbon allotropes Gaussian fitting around 1200 and 1550 cm^{-1} is the most spread fitting procedure [45] [46] [47] [48].

3.1.2 Experimental Data: As Deposited Material

For this thesis work Raman spectra of the as deposited material and of the annealed ones are perform with a visible excitation wavelength (532nm). The as deposited material show two broad peaks that are the convolution of several signals and a linear background attributed to photoluminescence, which comprises both fluorescence and phosphorescence phenomena and originates from an absorption/emission process between different electronic energy level in the material [49].

The presence of a strong background means that as deposited material is polymer like and that incorporate an amount of hydrogen, in fact the photoluminescence tends to increase with increasing on H concentration. Due to the saturation of non-radiative recombination sites through C-H bond termination and polymeric bond formation [50].

This is in agreement with the assumption of poly-acetylene presence on the as-deposited material coming from reaction of acetylene (C_2H_2) in plasma, during the deposition process on the reaction chamber.

For poly-acetylene the Raman fitting procedure lie on four Gaussian peak labelled μ_1 (≈1200 cm^{-1}), D (≈1350 cm^{-1}), μ_2 (≈1550 cm^{-1}) and G peak (≈1600 cm^{-1}), and is shown in figure 3.1.

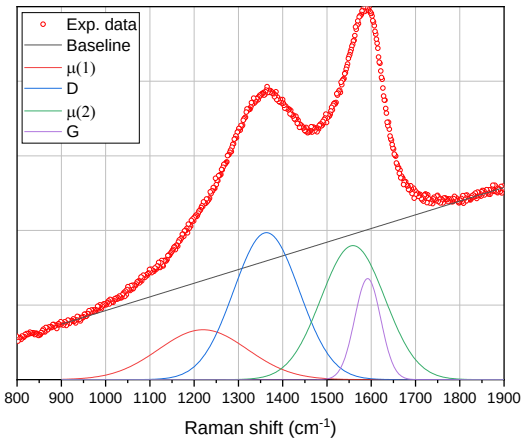

Figure 3.1: fitting procedure for as deposited material

3.1.3 Experimental Data: Annealed Material

For annealed samples, two different fitting procedure can be used. The first, used by Ferrari [42], is to fit the Raman spectra with four gaussian peaks at the same position of poly-acetylene. The assumption is that the material during annealing get pyrolyzed and become graphite, the graphitization evolution of the material during the thermal treatment is possible just by releasing hydrogen, this process is enhanced by the high vacuum reached for the thermal treatment (10^{-3} Pa), the releasing of hydrogen by pyrolysis of poly-acetylene, together with the surrounding amorphous carbon ordering, led to the formation of different structure made out only of carbon. In this case, the peaks μ_1 and μ_2 have a total different meaning: if for the poly-acetile those peaks are associated to the stretching of respectively C=C and C-C carbon, for annealed samples those peak are associated to carbo-nano onion (CNO) or some other carbon allotropes such as fullerenes and carbo-nano tubes, in particular μ_2 is attribute to the curvature of graphitic planes [51]. This fitting procedure can lead to some underestimation of the D and G peak since those peaks should be fitted by a Lorentzian

and BWF peaks respectively, the presence of a gaussian distribution just ahead of the peak at 1600 cm^{-1} decrease the intensity of this peak leading to unreliability of the quantitative information.

In figure 3.2 are shown the fitting Raman spectra with the procedure just described.

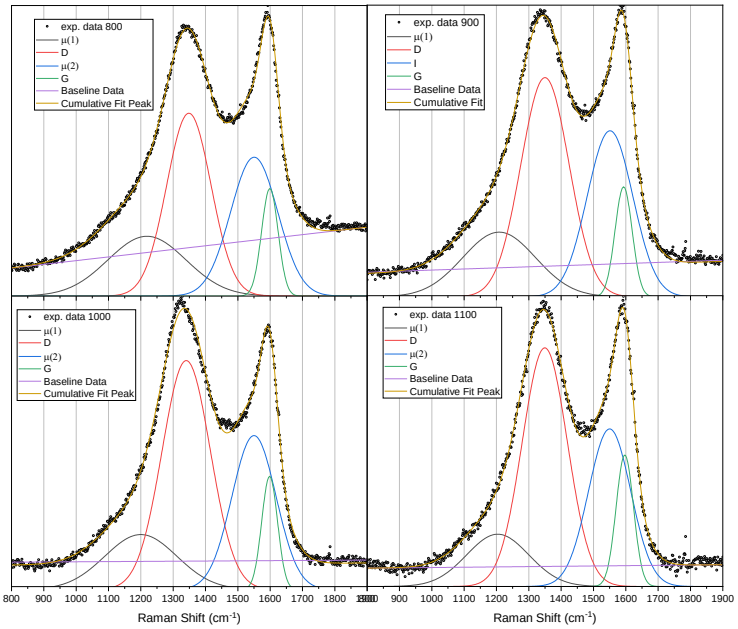

Figure 3.2: Raman spectra fitting procedure of the annealed samples, annealed temperature ranging from top left to bottom right

First evaluation on the Raman spectra fitting procedure is the presence of a baseline even at 800°C annealed temperature, this is an indication that not all the material undergoes graphitization and some tetrahedral carbon sp^3 is still present on the sample. The presence of hydrogen on the sample lower the formation of carbon allotropes possibility, even if from the Raman spectra, the presence of those carbon allotropes is verified.

The second procedure is to fit the Raman spectra with three peaks: Lorentzian for D, BWF for G peak and eventually, a gaussian for carbon allotropes added for the best fitting on the experimental data. In this case the supposition is to have a pyrolization and a graphitization process during the thermal treatment. By means of this procedure, the presence of carbon allotropes is subordinated to the formation of purely graphitic carbon structures, this approach is called bottom-up starting from the simplest structure assumption to

demonstration of the more particular one. In figure 3.3 are shown the fitting result for this second fitting procedure.

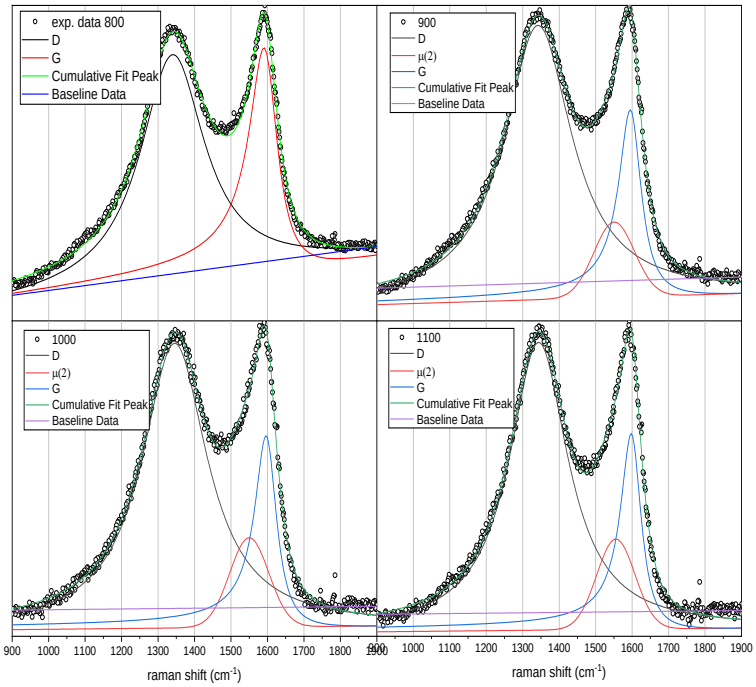

Figure 3.3: Raman fitting procedure for annealed samples, on top left the sample annealed at 800°C is clearly just a graphitic material with hydrogen contnent, for sample annealed at T>800 the just graphitic carbon structure does not suit anymore on the exp. data

As for the first fitting procedure, the baseline is attributed to photoluminescence and hence to hydrogen content and polymeric characteristic, in this case the just graphitic material assumption is acceptable for the sample annealed at 800°C while the Lorentzian and BWF fitting alone cannot describe fully the structure of samples annealed at temperature higher than 900°C. Hence, a description of their structure with just a graphitic material is not suitable, suggesting the presence of some carbon allotropes, emerging during the annealing.

The gaussian peak at 1550cm^{-1} is generally attributed to graphitic plane distortion, typical of carbon-nano onion and fullerene. The fitting of the D and G peak with a Lorentzian and BWF respectively give a better interpretation on the quantitative analysis of the materials.

3.1.4 Quantitative Analysis

The first parameter considered in the analysis is the position of G peak, a meaningful parameter in the Three Stage Model, proposed by Ferrari et al. [42], because related to disorder in the carbon phase. Following the ordering trajectory, G peak position goes from 1540 cm^{-1} in tetrahedral amorphous carbon, reaches 1600 cm^{-1} in nano-crystalline graphite and then decrease to 1580 cm^{-1} in perfect bulk graphite. Another consequence of increasing order is given by the I(D)/I(G) ratio, this value is related to defect number and crystal size, with a maximum theoretical value of 2,5 for a crystal size of 2nm . The growth of I(D)/I(G) over annealed temperature means that the carbon sp^2 is organized in ring and that the defects inside the material are increasing during thermal treatment [52].

In this work just the fitted curve with three peaks (bottom-up approach) are analyzed to have a lower underestimation of the values.

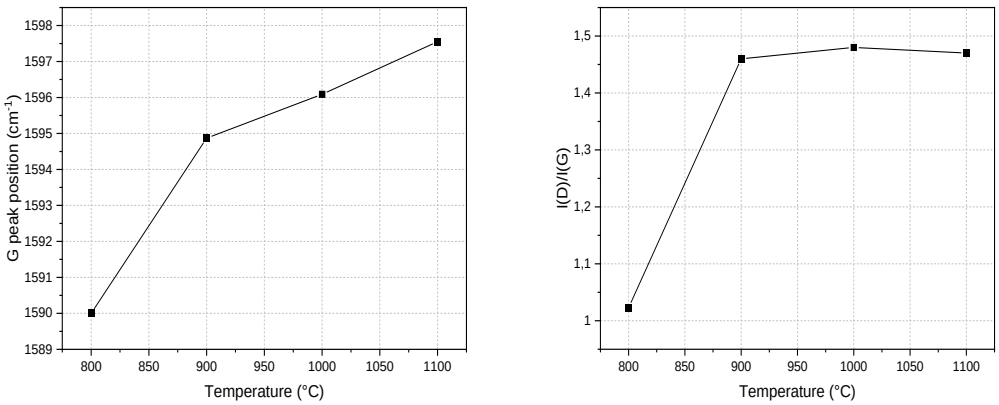

Figure 3.4: G peak position and I(D)/I(G) over the annealed temperature

are plotted the result from calculation of G peak position and D/G ratio. As can been seen in figure 3.4 the G peak position increase with annealing temperature, suggesting an increase on crystallinity domain during the thermal treatment. The presence and increasing intensity of the D peak can be probably correlated with the introduction of defects in the graphitic planes with high temperature. This is positive for the final electrochemical performance of the material, as it is known that the edges of graphite planes are the active sites towards vanadium ions redox reactions.

Another parameter analyzed is the slope of the baseline, normalized with the intensity of G peak *(I(G))*. In literature there are some empirical relation to correlate normalized slope

m/I(G) with hydrogen content. From figure 3.5 is notable how the baseline decrease from the as deposited material (marked as 0°C) until 1100°C this trend suggest that the material annealed at 800°C has some hydrogen-carbon bonded and hence some sp^3 hybridization carbon atoms.

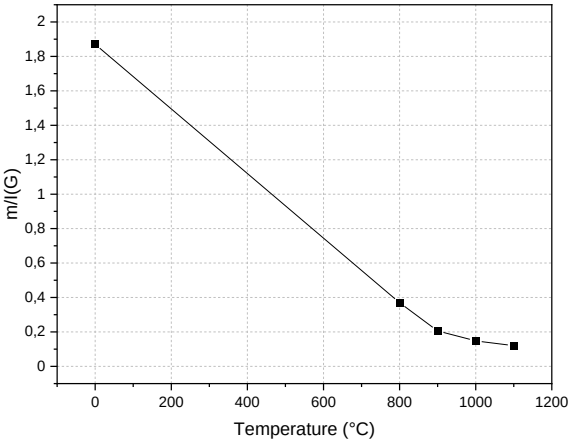

Figure 3.5: Raman baseline slope normalized on the I(G) peak

The last parameter considered in Raman fitting in the Full Width at Half Maximum (FWHM) (fig. 3.6): the FWHM of G peak is a parameter that is related to mean crystalline size. For fully crystalline NP the crystalline size equals to the particle size, so the analysis of FWHM(G) in our case is applicable only to annealed particles. In literature the FWHM have been already correlated with size, which in our case results to be between 5 and 10 nm.

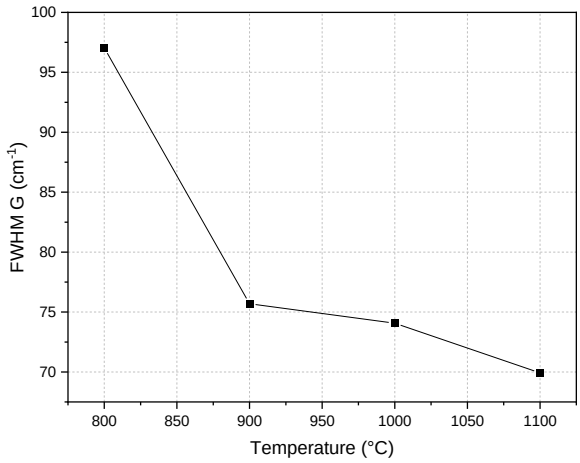

Figure 3.6: FWHM of the G peak over temperature of thermal treatment

As summary result of the Raman analysis is possible to demonstrate that the sample as deposited is almost just poly-acetylene, with high hydrogen content and low conductivity due to the high presence of sp^3 carbons.

For the annealed samples, during thermal treatment the material undergoes pyrolysis and start a graphitization process, at 800°C this process is not complete and so the material shown a little content of hydrogen on the sp^3 carbon, as indicate by the position of the G peak and *m/I(G)*, moreover the nanoparticles are major than 10nm. After 900°C, the material reach a maximum on carbon structure disorder as attributed by the I(D)/I(G) ratio, but the material continue to lower its hydrogen content and to shrink the nanoparticle size, this lead to formation of new all carbon structure with deflected graphitic plane (as suggest from the gaussian peak at 1550 cm^{-1}), increasing the disordering structure with a smaller crystalline size. Both the fitting procedure performed on the sample suggest the formation of carbon allotropes such as CNO or fullerene. Presence of such carbon allotropes should be confirmed by XPS analysis and/or HR-TEM image.

3.2 High Resolution TEM

High Resolution Trasmission Electron Microscopy technique is able to achieve extremely high magnification in order to capture even single atom image. For this thesis work High-resolution TEM images are acquired on an image-Cs-corrected JEM-2200FS (Schottky emitter), equipped with an in-column image filter (Ω-type), operated at 200 kV. HRTEM images were acquired using a direct electron detection camera (K2 Summit, Gatan), in super

resolution mode. Each image shown here is obtained from a (260 nm)2 frame resulting from the sum of aligned 30-40 frames obtained by short exposure (0.3-0.4 s), with a total acquisition time of 12 s. Sample preparation consist in powders of nanostructured carbon suspended in ethanol, sonicated shortly and supernatant drop-cast onto holey-carbon-coated Cu grid.

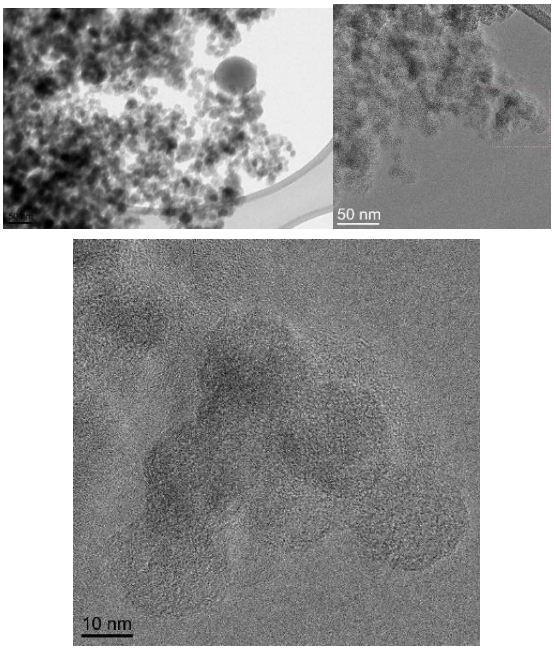

Figure 3.7: HR-TEM of sample annealed at 800°C

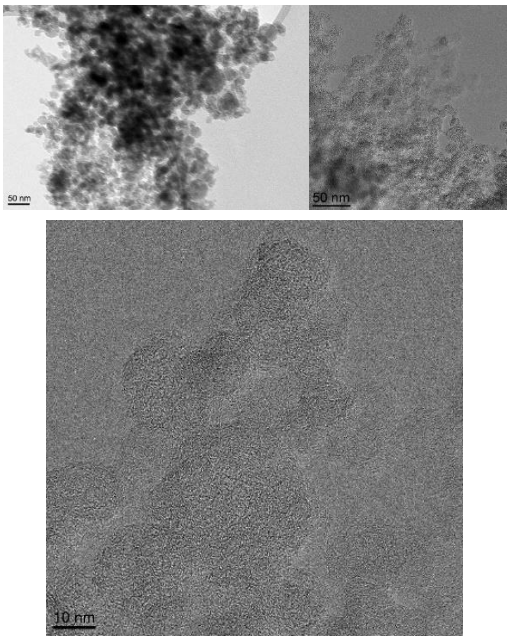

Figure 3.8: HR-TEM of sample annealed at 900°C

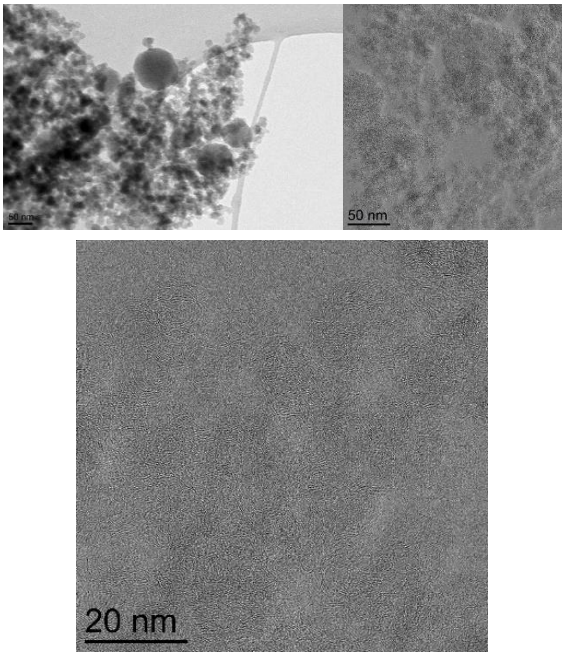

Figure 3.9: HR-TEM of sample annealed at 1000°C

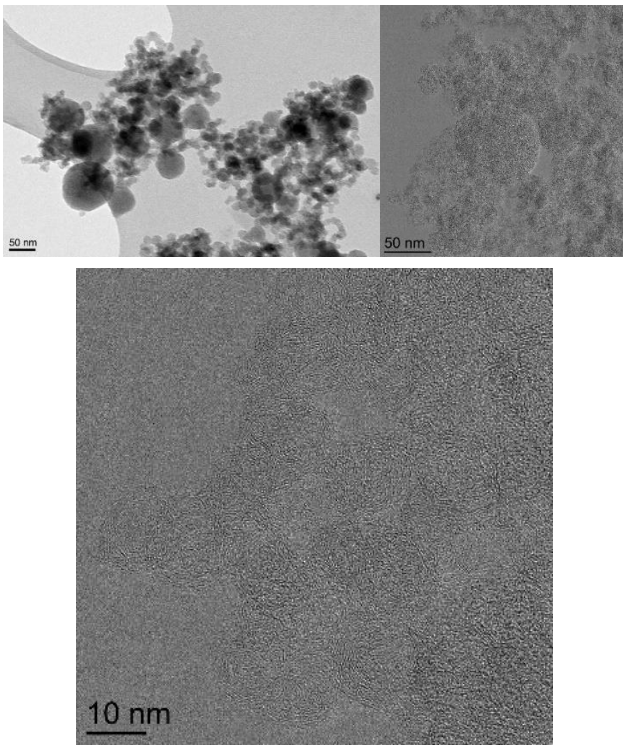

Figure 3.10: HR-TEM of sample annealed at 1100°C

HRTEM analyses of samples annealed at temperatures ≥1000°C exhibit some irregular shell-like features, with an inter-spacing close to 3.4 Å (spacing between (002) planes of graphite, typically observed in carbon nano-onions).

Moreover, from HRTEM is possible to identify together with the few nm-sized carbon particles, larger globular particles of approximately 50 nm in increasing fraction with increasing annealing temperature. This trend of increasing large particle fraction could be attribute to film density: larger particles will arrange in an more open structure than lower particles.

The formation of Carbon Nano-Onion like structure at 1000°C is in accordance with the Raman fitting procedure (bottom-up approach) proposed, the ordering ring trajectory start around 1000°C.

3.3 SEM & Film Morphology

A Scanning Electron Microscope is a microscopy technique that produces high resolution images of a sample surface. It exploits a focused electron beam that scans the analyzed

surface. Electrons hitting the sample exchange their kinetic energy through many kinds of physical processes. Secondary electrons (SE), generated as ionization products, possess low energy and come from within a few nanometers below the surface. They constitute the main means of viewing images in the SEM, highlighting morphology and topography. The other output signals that are produced are: backscattered electrons (BSE), diffracted backscattered electrons, Auger electrons, elastically-scattered electrons, characteristic and bremsstrahlung X-rays, visible light (through cathodoluminescence) and heat. They are all a source of meaningful information, depending on the sample under investigation and the purpose of the analysis. One can even extract information about the chemical composition of the sample and the elemental distribution.

SEM must operate under high vacuum and the analyzed samples must be electrically conductive, dry and clean. The magnification level can be as high as 10^6x, with a resolution that can reach 1 nm.

3.3.1 Film Density

Film density have been investigated by gravimetric method: NPs have been deposited on silicon substrate, previously weighted, to calculate the mass deposition rate. Film thickness has been evaluated with SEM image to calculate the thickness deposition rate and to evaluate the density of the porous film.

In order to lower the error on the measure a thick deposition of one hour has been performed. Thickness uniformity over the slit line is not guarantee but a good thickness uniformity is out of the scope of this thesis work, thickness uniformity is mainly governed by the diffusor porosity, during different deposition some pores may be obstruct and uniform distribution of the reactant inside the reaction chamber may vary . In order to eliminate the error due to comparison of samples positioned under different slit position, a matrix on the sample holder have been made. Each row of the matrix has been annealed at a different temperature and comparison of the sample annealed at different temperature are made by their column position on the sample holder (fig.3.11).

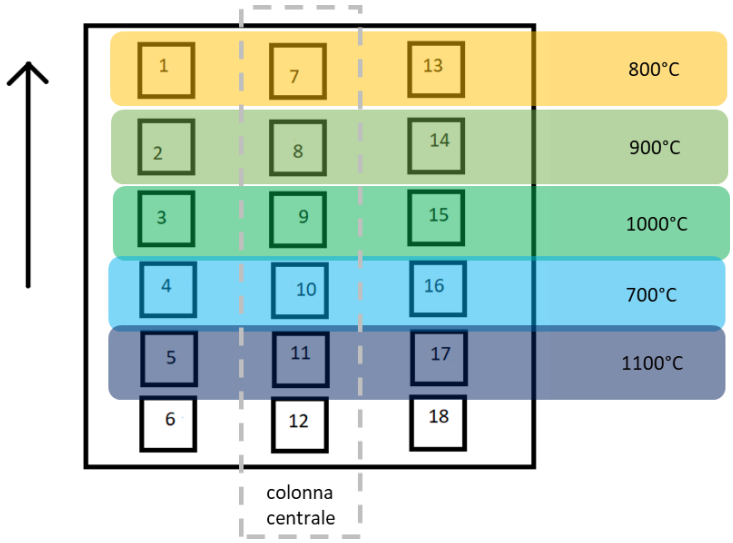

Figure 3.11: Matrix of the deposition for density analysis

Gravimetric study on the as deposited and annealed sample (fig. 3.12) shown that the mass loss after the annealing procedure is the same for all the temperature, the value is set around 30% of mass loss.

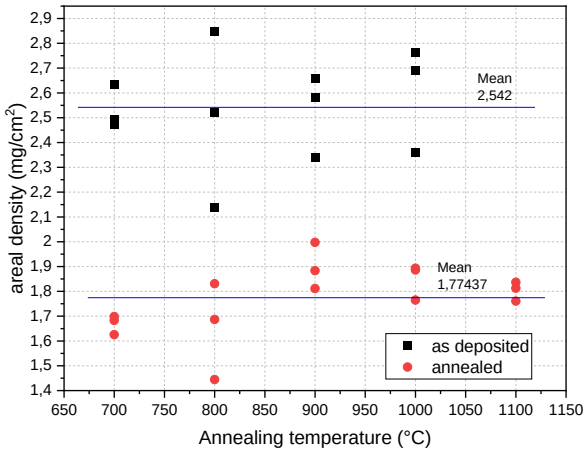

Figure 3.12: Aereal mass of as deposited and annealed sample

Areal mass can be converted to mass deposition rate since the deposition time is a constant. A mean value of ~42 µg $cm^{-2}min^{-1}$ has been calculated for the as deposition process with parameter as defined in section 2.5.

From the thickness analysis performed by SEM image of the annealed samples (fig. 3.13), is clearly visible that even if we have a releasing of hydrogen content during the thermal annealing as check from the Raman spectroscopy (fig. 3.5), the material does not densify itself but rather it shown an increasing trend of thickness and hence a decreasing of density, leading to a more open porosity material with high degree of graphitization and the presence of carbon allotropes.

Density, together with average pore size determine the mass transport properties of a porous electrode.

For the sample annealed at 1000°C the lowest density and higher thickness is reached, this can dramatically increase the available surface for reaction with vanadium ions and mass transport inside the electrode. Over 1000°C the suggestion is the material nanostructure start to collapse decreasing the nominal thickness and increasing in density.

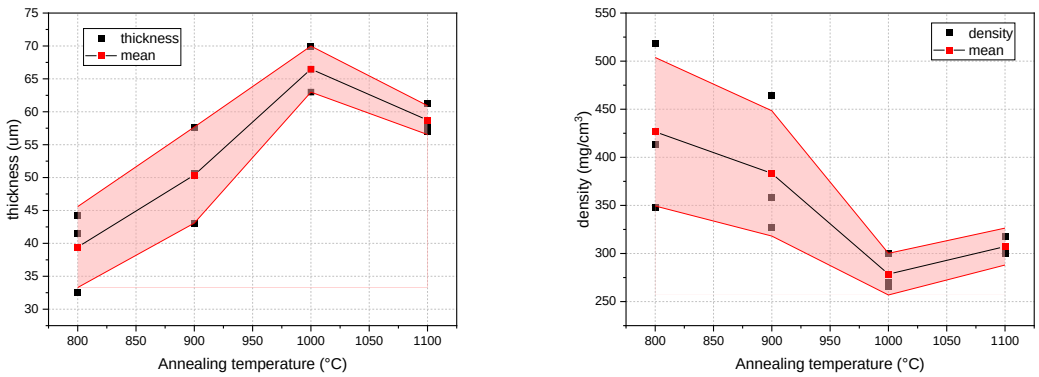

Figure 3.13: thickness from cross section of annealed material and density at different temperature

3.3.2 Film Morphology

Since the as deposited material is poly-acetylene it has not a good conductivity, thus is difficult to have a good magnification and resolution of the SEM image (fig. 3.14). A good adherence to the substrate can be observed, and the structure looks compact at this level of

magnification. Unfortunately, the electrical conductivity was too low to get meaningful top-view images. After the annealing process, nanoparticles are expected to undergo graphitization, increasing their electrical conductivity. As a result, it is easier to get better-focused pictures at high magnifications.

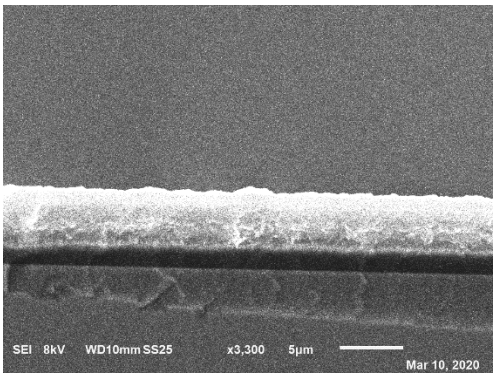

Figure 3.14: SEM cross section of as deposited material

As can be seen on figure 3.15 and 3.16 the annealed material forms a network of attached particles with a porous structure, the nanoparticle diameter is measure around 10nm as expected from Raman analysis.

For annealed sample at T>800°C the morphological structure of the nanoparticles is not influenced, with the loss of hydrogen, shrinkage and deformation of graphitic plane the structure of the particles become more circular.

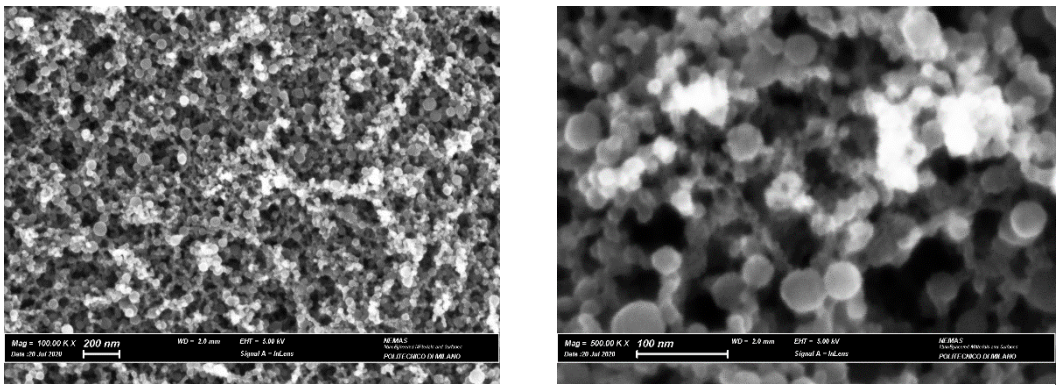

Figure 3.15: SEM image at high magnification of annealed sample at 900°C, 100K X magnification on the left and 500K X on the right

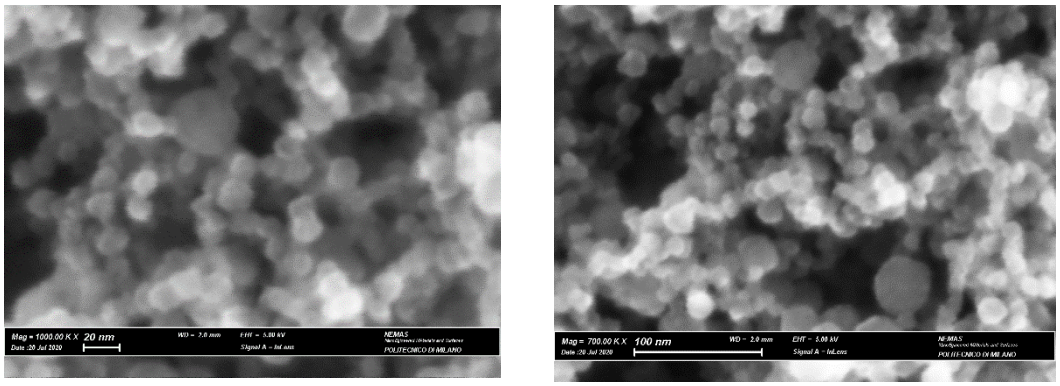

Figure 3.16: SEM image high magnification of sample annealed at 1000°C, on the left 1000K X, on the right 700K X magnification

At the SEM image all the annealed sample over 900°C seem to show all the same open porosity, no information on carbon allotropes presence can be extrapolate from SEM image since the structure dimension are much lower than the SEM magnification.

No information of high magnification cross section SEM of the annealed sample is present in this thesis work.

3.4 XPS

The working principle of a X-Ray Photoelectron Spectroscopy (XPS) is based on two different effect that can take place when a sample is irradiated with a monochromatic X-ray source, namely photoelectron effect and Auger emission which are indicative of valence electrons and core electrons respectively. In both cases an electron is expelled from the material and its kinetic energy is measured. The bonding Energy (E_B) can be calculated as:

$$E_B = h\nu - K - \phi$$

Where hν is the energy of the incident photons and ϕ is the work function of the spectrometer. XPS can give only information regarding superficial layers of sample (few nanometers deep), because electrons coming from deeper layers would lose their kinetic energy. No information on hydrogen content is obtainable from XPS analysis.

3.4.1 Experimental Data

XPS analysis has been performed in this thesis work to obtain information about atomic %, presence of contaminant and ratio of sp^2/sp^3 carbon atoms on annealed sample ranging from 800°C to 1100°C. The entire spectra obtained has been better analyzed to understand the chemistry of the contaminant present on the samples.

On figure 3.17 is present the wide scans of the annealed samples and the table of atomic % content, oxygen at the surface could come from exposure to air of the annealed sample or during the thermal treatment procedure. Presence of nitrogen on the sample is unexpected, figure 3.18 shown the nitrogen and carbon spectra, the Nitrogen spectra could be decomposed into 5 components (a-e), assigned to different N coordination with C. The main peak, a and c, could be assigned to pyridinic and pyrrolic N respectively. The increase of the annealing temperature mainly affects the pyridinic one, whose intensity decrease faster than that of the pyrrolic one.

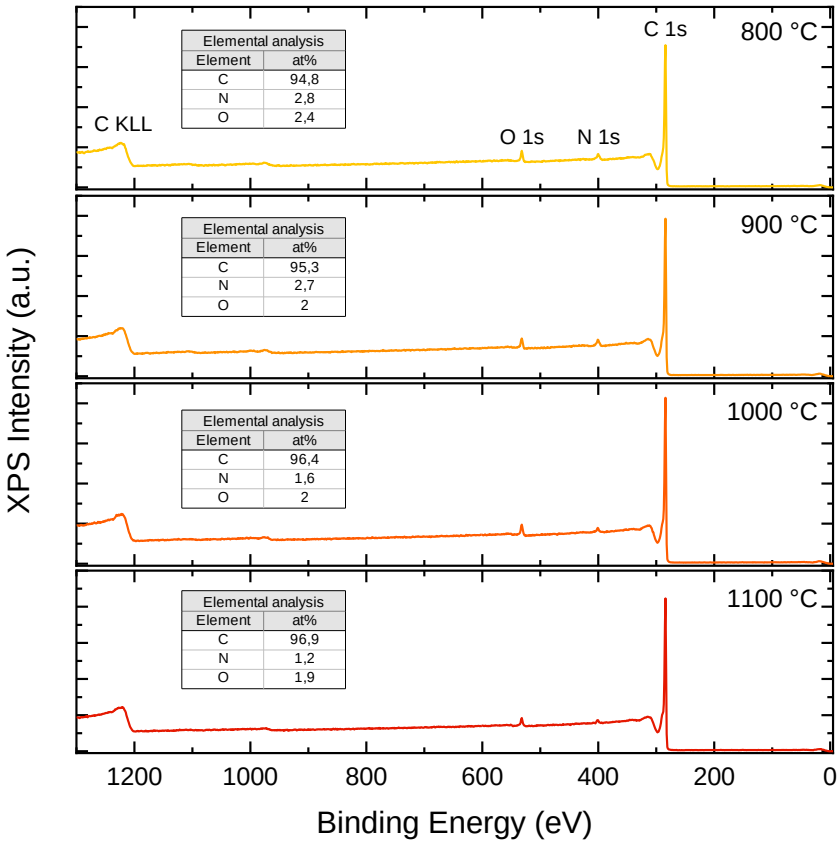

Figure 3.17: XPS wide scan and table of atoms content

The main procedure to introduce nitrogen coordinated C, is by plasma reaction, so to justify nitrogen presence the assumption is that a leak during the deposition is present on the NanoJeD system, more in detail the leak should be present on the line that connect the glovebox (in N_2) to the NanoJeD.

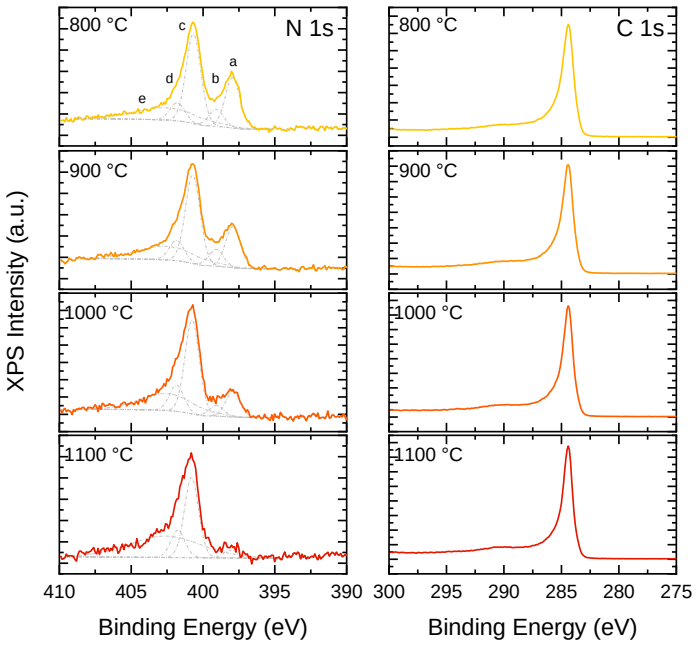

Figure 3.18: XPS spectra focus on the N1s and C1s regions

For a good fitting procedure of the carbon peaks, assumption on two different typologies of sp^2 carbon must be considered, their concentration evolves in relation to the annealing temperature. The two assumed peaks are relative to flat and curve graphitic planes. In table 3.1 are shown the relative concentration of those two peaks, “carbon A” is assigned to the curve graphitic plane, typical of fullerene and CNO.

	Carbon A	**Carbon B**
800°C	43.6%	56.4%
900°C	51.8%	48.2%
1000°C	56.7%	43.3%
1100°C	56.8%	43.2%

Table 3.1: relative concentration of sp^2 carbon type allotrope

Table 3.1 would propose a presence of carbon allotrope even the sample annealed ay 800°C, but the XPS analysis does not give information on the hydrogen content and so to the information on the sp^3 presence are not easily obtainable. Shape of the C KLL Auger spectrum (fig 3.19) provides a measure of C sp^2/sp^3 hybridization. C sp^2/sp^3 content is evaluated from parameter D, which is defined as the energy difference between the maximum and minimum of the first-derivative C KLL spectrum, where dependence of parameter D on C sp^2/sp^3 hybridization is assumed to be linear the D values of graphite (approx. 22 eV, depending on crystallinity and grain size) and diamond (approx. 13 eV). The presence of oxygen decreases the value of the D-parameter [53].

Considering that the oxygen content of the investigated samples is approximatively 2%, the observed D-parameter values are consistent with sp^2 hybridization of carbon at all the annealed samples.

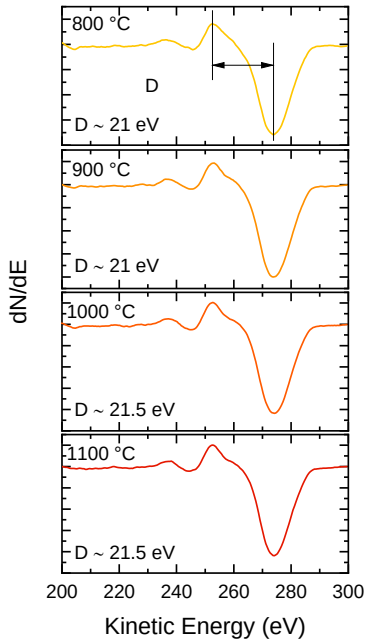

Figure 3.19: C KLL Auger spectrum of different annealed temperature samples

In figure 3.20 are plotted the result of the table 3.1, the graph shown that, assuming a graphitic material at all the temperature with differences on the carbon allotropes relative concentration, a plateau of fullerene/CNO relative concentration is reached at 1000°C.

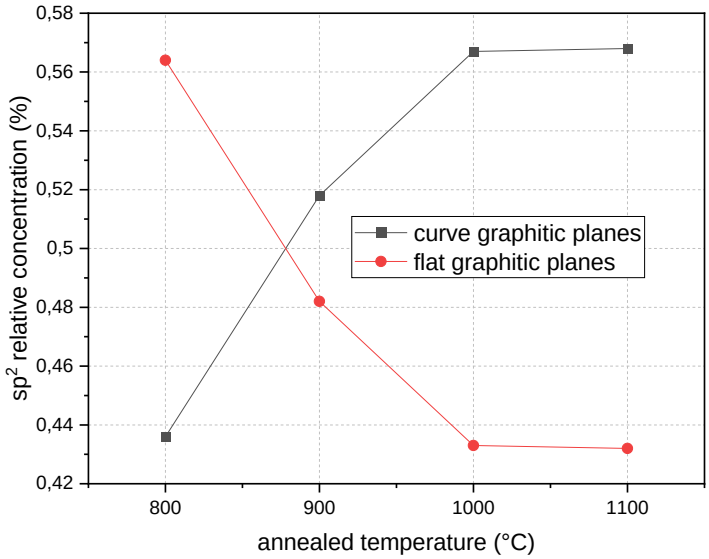

Figure 3.20: relative concentration of different type of graphitic planes

Nitrogen-doped graphitic carbon electrode porous material for VRFB is well known to enhance the catalytic performances, in particular the mechanism is based on the negative charge density of incorporated N atoms: due to their strong electronegativity, the adsorption process of positively charged ions is promoted. Then, the formation of a transitional N – V bonding state facilitates the charge transfer between the electrode and vanadium ions [54]. Also oxygen content increases the catalytic performance of the electrodes.

Content of oxygen and nitrogen decrease in relation to the increasing of annealed temperature, so catalytic affinity toward vanadium redox reaction should decrease in function of the temperature, while increasing thermal treatment temperature the material start increase the graphitic percentage and increase the carbon allotropes presence. Only a study on the electrode performance can understand which of those two effects has a larger effect on the vanadium redox flow battery efficiency.

Chapter 4
Electrochemistry Of Carbon Films For Vanadium Redox Reaction

In the previous section, chemical and morphological information regarding the material and the connection with the thermal treatment parameter has been established, concluding that annealed particles have high conductivity and maximized number of active sites, in particular the sample annealed at 1000°C show an open porosity and a morphology ideally suitable for mass transport of vanadium electrolyte inside the electrode. Now is important to electrochemically test those material in order to verify if the hypotheses based on the observer properties find some correspondence with the electrochemical behavior of the electrodes.

The established technique to probe electrochemical electrodes' performance is the cyclic voltammetry measurement, where the sample is tested in a three-electrode cell set-up. CV's give information about the goodness of an electrode toward a single reaction of oxidation and reduction separately removing mass transport issues not related to electrodes (ion cross-over etc.).

The material for CV test has been deposited on a glassy carbon surface since silicon substrate is nonconductive and so not suitable for this kind of test. After CV test, the material has been deposited on a carbon paper GDL 39AA, with a nominal thickness of 299 microns and tested first in a symmetric cell and subsequently in a segmented full cell in order to have a response of the material at the real operational condition of a vanadium redox flow battery. The tests have been performed using a Nafion 115 membrane and different low field. For symmetric cell test, electrode overpotential and kinetic parameter trends such as cathodic transfer coefficient α_c and exchange current i_0* has been evaluated at different temperature, calculation of such value is not possible due to impossibility of decoupling the concentration overpotential to the kinetic one. For full cell test energetic, columbic and voltaic efficiency have been calculated.

4.1 Cyclic Voltammetric Analysis

The cyclic voltammetry analysis is carried out in a three-electrode cell set-up, schematized in figure 4.1. In this configuration a working electrode, a counter electrode and a reference electrode are immerse in the electrolyte solution consisted in a 2M sulfuric acid and 0,1M Vanadium V^{3+}, the choice of V^{3+} has been done in order to have a State Of Charge (SOC) equal to 0%. Since the production of current depend on the amount of vanadium redox reaction occurring at the electrode, it is function of the area expose to the electrolyte, in order to compare different material annealed at different temperature, excluding the exposed area factor, Teflon tape has been applied to mask the film leaving a known area of 0,2 cm^2 open to the reaction. The counter electrode used for this test is a GDL made of carbon paper 29AA, which has been chosen for its known electrochemical activity toward vanadium ion redox reactions, counter electrode area has to be major than the working one in order to guarantee the maintenance of the SOC. The refence electrode used is a calomel electrode (E_0 = +0,197 Vs. SHE), all the cyclic voltammetry plot has been normalized to SHE.

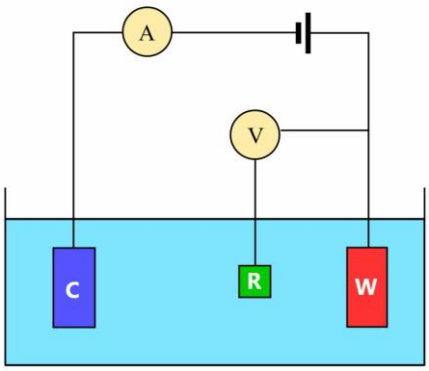

Figure 4.1: schematics of the three-electrode cell setup [33]

The three-electrode cell configuration is necessary because the potential of the working electrode, where a current is flowing, cannot, in general, be determined by measurements with respect to the other current-carrying electrode in the cell (counter electrode). A third electrode must be introduced as a reference. A high-impedance voltmeter ensures that no significant current passes through the reference electrode in order to avoid any overpotential

contribution. With this specific setup it is possible to investigate separately positive and negative vanadium ions redox reactions. Cyclic voltammetry consists in apply a triangular cycling potential to the working electrode with respect to reference measuring the produced current. When the electrode potential exceeds the potential of a certain reaction possible in the electrolyte, current density ramp up or down on dependence of an oxidation or reduction reaction.

In this work 10 cycles are been done for each electrode and just the 10th cycle has been compared in order to reach a steady-state of the performance.

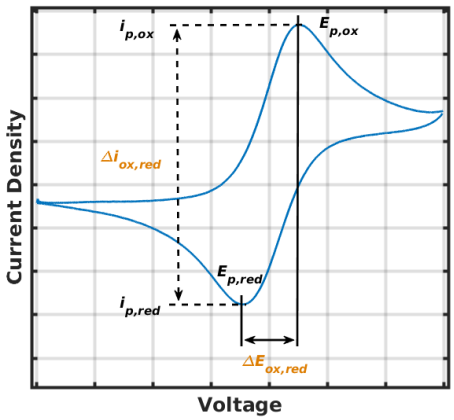

Figure 4.2: Scheme of a generic CV plot (picture taken from [33])

In a generic CV plot (fig. 4.2) two peaks are present, one responsible of the oxidation and one of reduction of the species. The value observed in a CV plot are the peaks position and peaks height: the separation of the peak potential ($\Delta E_{ox,red}$) indicate the potential difference needed to drive the redox reaction, while the difference in peaks height ($\Delta I_{ox,red}$) evaluate the maximum current density generate from the cell, closer the peak position and higher the difference in term of current densities, better is the electrode activity.

For a correct interpretation of the CV is important to separate the different contribution such as redox kinetics, side reaction kinetics, double layer capacitance and charge transport. Some contribution, such as resistivity of cable and double layer capacitance, can be evaluate and subtracted to the original CV plot in order to isolate only the part regarding the redox kinetic. The procedure for evaluation and subtraction of cable resistivity is called iR correction, this correction has not been done for this CV performance.

$$V_{IR\,corr} = V_{exp} - R_{\Omega} \cdot I$$

For identify other type of contribution, such as double layer capacitance and charge transport a CV should be performed in a 4M solution of H_2SO_4, no presence of active species in the ranging potential permit to just electrostatically charge the electrode and study the contribution of double layer. In this CV analysis, just the negative side (anode) of the vanadium redox flow battery have been tested, no study on double layer capacitance have been performed.

In the negative redox reaction of a VRFB, vanadium ions in oxidation states V^{2+} and V^{3+} react on the edge of graphitic plane of the electrode, the equilibrium potential depend on SOC of the battery as describe by the Nernst equation:

$$E = E_0 + \frac{RT}{F} ln \frac{V^{3+}}{V^{2+}}$$

Equilibrium potential range from -0.15 to -0.35 V

4.1.1 Experimental Result

Cyclic voltammetry experiments output (i-V) are affected by the scan rate, in particular the maximum current density value depend linearly on the square root of the scan rate, while the peaks distance (ΔE) slightly increase with the square root of scan rate. All the CV in this work are been taken at a scan rate of 100 mV/sec.

In figure 4.3 are present the cyclic voltammetry analysis of different sample annealed at the temperature of interest, difference in the cycles are not easily detectable. Is Possible to notice that the material annealed at 1100°c slightly diverge from the form of the other temperature, in particular the material annealed at 1100°C shown a catalytic effect to the hydrogen evolution reaction at lower potential, moreover the cycle is shifted downward, thus generating more current but not from vanadium redox reaction.

A better performance comparison is noticeable through the index of merit called ΔE and I_{ox}/I_{red} shown in figure 4.4. Here the different are evident, the material annealed at 1000°C shown the best performance in term of catalytic activity toward Vanadium redox: a small ΔE allows for a reduction of the charge voltage, increasing the voltaic efficiency. For a good interpretation of the result, cross-check with physical and morphologic properties (chapter

3) should be done. Increasing thickness a higher total surface area is expected increasing the available area for reaction, as shown in fig.3.8 starting from the same deposition, the material annealed at 1000°C show the larger thickness and lower porosity, those parameters influence the mass transport and kinetic of the electrode.

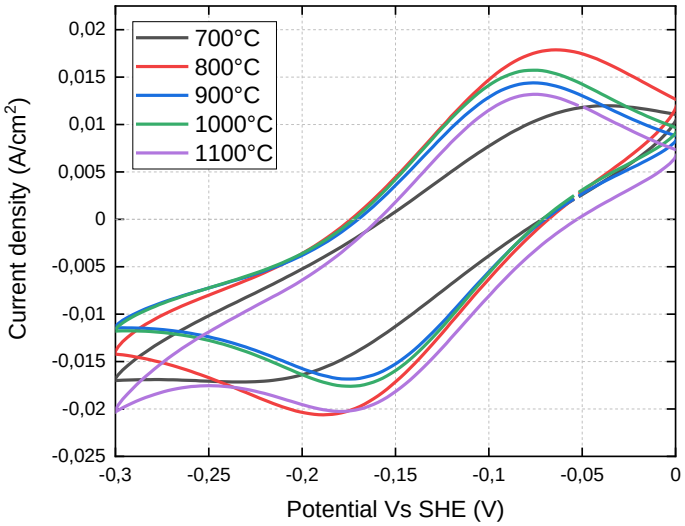

Figure 4.3: Cyclic voltammetry plot of different annealed temperature

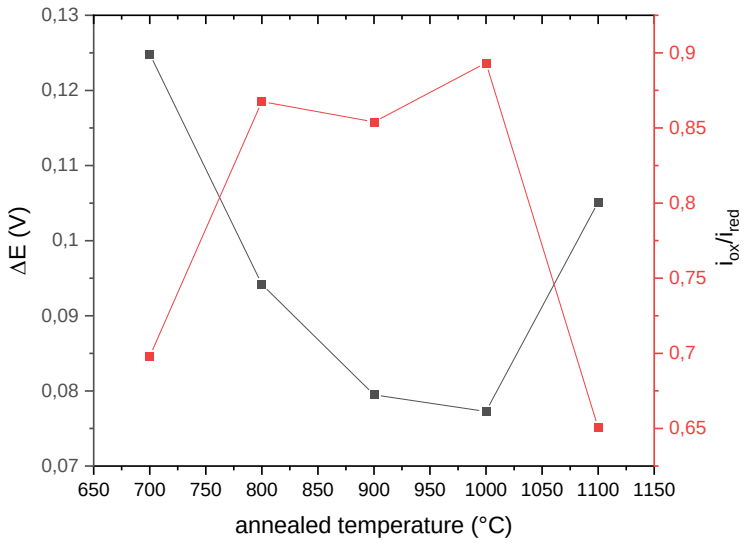

Figure 4.4: calculated index of merit ΔE and Iox/Ired vs temperature of annealing

4.2 Symmetric Cell Test

For real performance test, the carbon nanostructured material has been deposited onto the GDL Sigracet 39AA, fabricated with electrospinning technique. In order to investigate the different fluid-dynamics performances two different flow field distribution have been tested: serpentine and interdigitate (fig. 4.5).

In order to decouple the different losses contribution rising from the complex geometry of the cell, the fluid-dynamics and the cross-over coming from the ion exchange membrane and precisely assess the NP deposition effect, a different cell set-up is used to investigate just the negative electrode, that suffer of the sluggish kinetic and so is the limiting electrode of the VRFB, a symmetric cell have been built where the same electrolyte is used at both half-cells. Electrolyte is pumped from the reservoir into one side of the cell where oxidation reaction occur, that the same electrolyte is pumped to the other side of cell where reduction reaction occur, this permit to maintain the same SOC that should be fix at 50% in order to don't boost the reaction on one side of the cell respect the other. The recirculation of the same electrolyte allows also to eliminate crossover contamination. A schematic view of the symmetric cell configuration is exploited at figure 4.6.

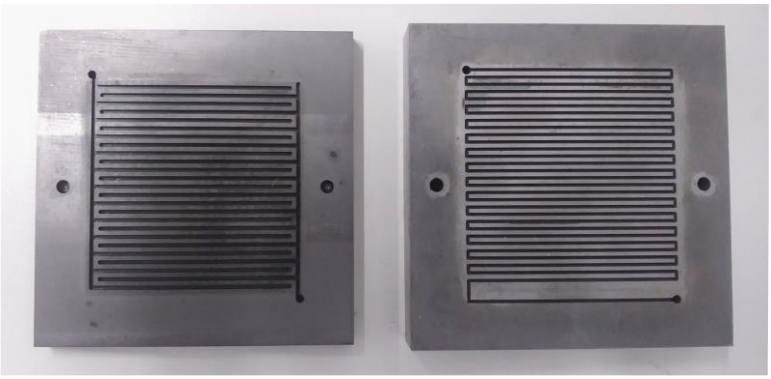

Figure 4.5: picture of interdigit (left) and serpentine (right) flow field distribution

All the tests are performed using 1M vanadium in 4M sulfuric acid, electrodes are separate by Nafion 115 membrane boiled before cell's assembly, the cell area is determined by gaskets that help to seal the cell. All the electrodes are prepared by same deposition process, time and swept, the difference rise from the annealing treatment. Since after annealing the electrodes show different thickness and different density, some legit doubts regarding the electrodes comparison may rise: for electrochemical performance the important parameter is the mass, to asses if an electrode show the best performance compare to other is important

to keep the mass equal so to highlight only the morphology difference, in this case mass reduction after annealing is evaluate of 30% independently on the annealing temperature, so comparison of electrodes coming from the same deposition are acceptable.

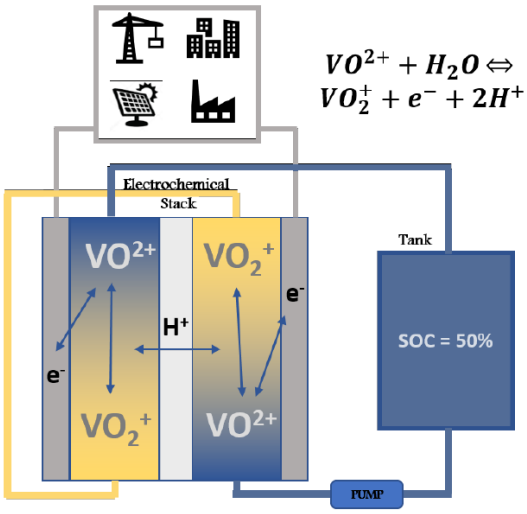

Figure 4.6: schematic figure of a symmetric cell set-up [32]

4.2.1 Experimental Data

The use of symmetric cell allows to have a stable and reproducible working condition, avoid capacity fade due to cross-over and SOC variation. Voltage limits for oxidation and reduction reaction has been imposed in order to avoid side reaction as HER and carbon corrosion, characterizing electrodes performance in the same range where they will operate in charge-discharge cycles. After assessing that the electrodes have a better performance than the reference electrode compose of just carbon paper 39AA (fig.4.7), polarization curve have been performed at different flow rate in order to identify kinetics and mass transport limiting phenomena. By increasing flow rate, limiting current and overall cell performance increase as there is a reduction in mass transport losses leaving kinetics to be the dominant phenomenon, flow rate also contributes to pumping losses and generation of high mechanical stresses on carbon fiber. An optimization on the generated power respect the required from pump alimentation should be considered during design of a VRFB system, in this case the goal is the study of electrode overpotential rather that net power generation and so the best flux performance have been verify with the 100mL/min. 80mL/min plot have been investigate for confrontation with the reference untreated electrode.

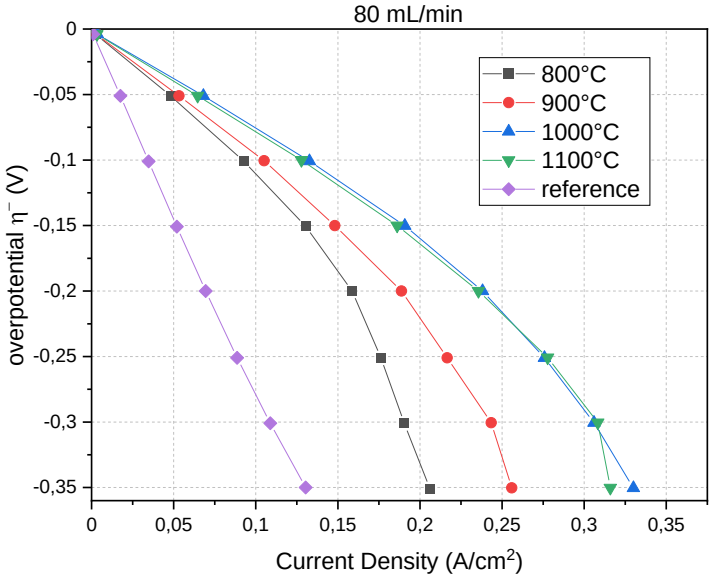

Figure 4.7: polarization curve of electrodes referred to reference electrode (GDL), performed at 80mL/min with interdigitated flow field

In figure 4.8 are shown the performance of different electrodes annealed at different temperature, the experiment has been performed at the maximum flow rate reachable for the pump used (100mL/min). The best performance fall on the sample annealed at 1000°C, that is the one with lower density and higher thickness but with the same mass of other annealed samples, demonstrating that the concentration of carbon allotropes and morphology is fundamental for a good performance rather that the nitrogen or oxygen content.

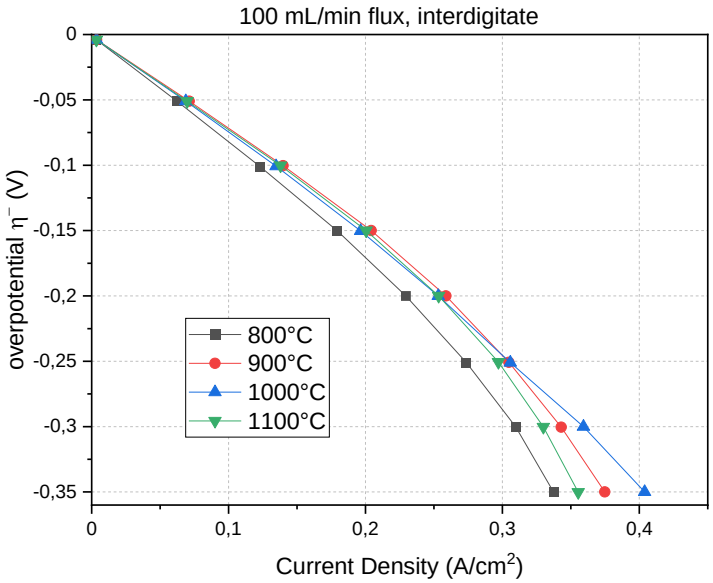

Figure 4.8: Polarization curve of different annealed electrodes

At the end, a different flow field has been tested for the best performed electrode. In this case the utilization of a serpentine flow field enhances the performance of the electrode: the influence of the flow field is affected by various physical parameters, such as the active area of the cell, the electrode porosity and permeability, and the stoichiometry of the reactants. Moreover, there is a strong interplay among these physical quantities. There is not a standardized optimum flow field in the benchmark, the performance vary in dependence of the used electrode, for example: Zago et al. in [55] used the SIGRACET 39AA Carbon Paper as electrode, and they reach the best performance using a serpentine flow field, while in Zhao et al. in [56] used a modified Graphite Felt as electrode and the best perform have been obtained with the interdigitated ones.

In this case, as in [55] where carbon paper 39AA was tested, the best performance are obtainable with the introduction of the serpentine flow field, polarization curves are shown in figure 4.9

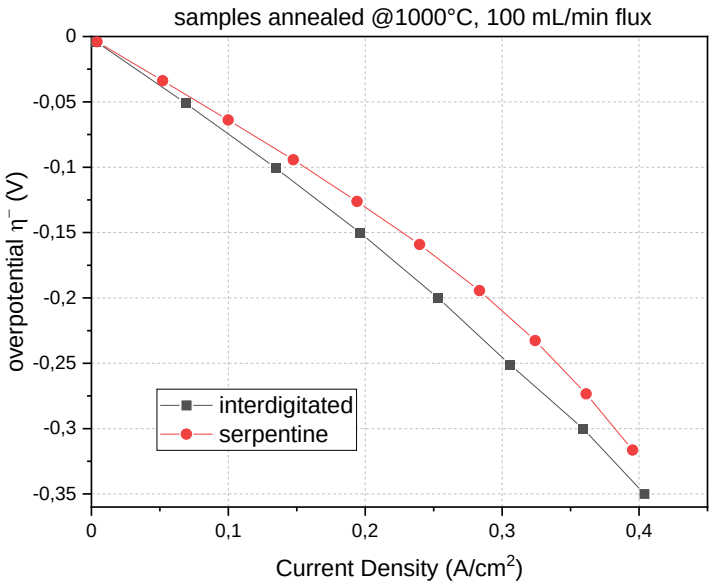

Figure 4.9: Polarization curve interdigitate flow field vs serpentine

4.2.2 Kinetic Analysis

Since the result output of the symmetric cell test is a polarization curve, in figure 4.10 is shown the Butler-Volmer fitting curve, such plot converges to the Tafel equation at high overpotential. From Tafel equation could be possible to extrapolate some important physical parameter such as the exchange current density (i_0*), transfer coefficient α and reaction rate coefficient *K*. Those parameter are detectable only when the activation overpotential is the dominant one, in this case ohmic overpotential have been simply subtracted from the total overpotential but concentration overpotential cannot be considered negligible at high current densities and for its estimation study on the limiting current I_{lim} by LSV or CV with rotating electrode should be performed. Since the same electrode is use at the both part of the cell and by assumption on transfer coefficient equal to 0,5 for the reaction V^{3+}/V^{2+}, the overpotential can be divided by two to identify the electrode overpotential of one side of the symmetric cell. Furthermore, assumption of equal rate of reaction for oxidation and reduction must be considered.

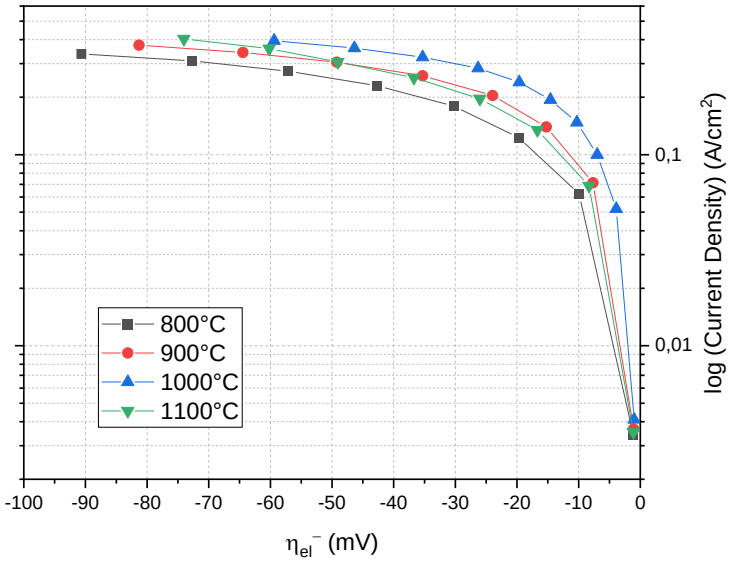

Figure 4.10: Tafel fitting for V^{2+}/V^{3+} for GDL with carbon NP annealed at different temperature

Exchange current density value the electrochemical activity of the electrode toward the redox reaction [57], while transfer coefficient predict the symmetry of reaction energy barrier, a value of 0,5 means a perfectly symmetrical energy barrier to overcome for starting the reaction. [58].

The outperformed electrode has been compared to the reference untreated one (fig.4.11), the electrode overpotential result is the sum of activation overpotential and concentration overpotential.

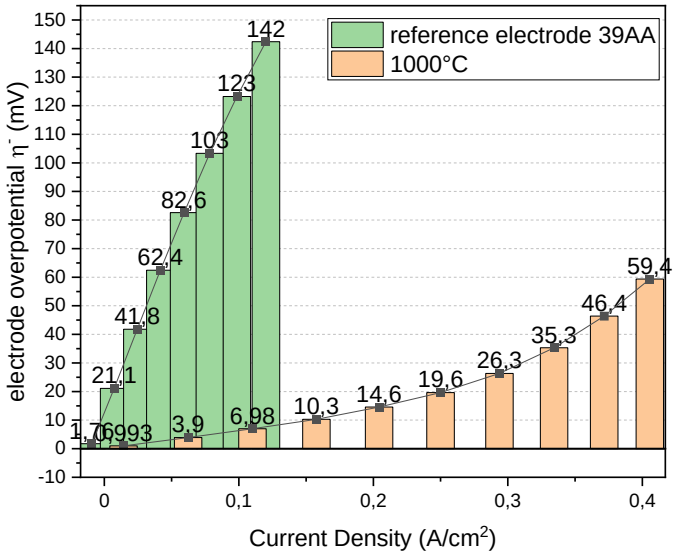

Figure 4.11: electrodes overpotential Vs current density

Electrode overpotential has been estimated to be around 60mV for a high current density such as 400mA/cm^2, considering that the negative electrode suffers of the sluggish kinetic [59], comparing the Carbon nanostructured electrode with the commercial one an overpotential of just 60mV is an outstanding result.

4.3 Full VRFB Cell Test

From the symmetric cell characterization and cyclic voltammetry has been possible to identify the best annealed temperature for implementation of carbon-based nanostructured material as electrode. Test in a segmented VRFB full cell with serpentine flow field, which proved to be the best suitable one, has been performed imposing a current density over the electrode and measuring the tension between anode and cathode. An electrolyte volume of 50mL has been used and kept in 3bar nitrogen inert atmosphere to prevent vanadium oxidation.

Segmented cell permit to measure the polarization curve in each part of the electrode, analyzing locally the mass transports and kinetics phenomena [60], in this work has been use a segmented cell hardware of 25cm^2. In figure 4.12 is shown a schematic view of a segmented flow battery scheme. In all the experiments electrodes annealed only at 1000°C

have been tested, cell performance is evaluated through efficient index such as coulombic efficiency, voltaic efficiency and energetic efficiency.

Coulombic efficiency, measuring the exchanged charges between the discharge and charge phase of the cycles.

$$\eta_c = \frac{C_{discharge}}{C_{charge}} = \frac{I\ x\ \Delta t_{discharge}}{I\ x\ \Delta t_{charge}} = \frac{\Delta t_{discharge}}{\Delta t_{charge}}$$

In general charge and discharge current are the same, so the coulombic efficiency is simply the ratio between discharge over charge times. Coulombic efficiency account for all losses generating capacity fade such as ion cross-over, self-discharge and secondary electrode degradation. Voltaic efficiency is defined as the ratio of the average voltage during discharge and charge:

$$\eta_V = \frac{\bar{V}_{discharge}}{\bar{V}_{charge}}$$

Voltaic efficiency takes into consideration the average cell voltage, a quantity accounting for ionic losses (membrane), mass transport (flow rate, type of flow field) and electrodes. To point out the aspect related to the redox kinetics and mass transport only, the iR corrected η_V is the right indicator, representing only electrode's properties. The energy efficiency is the ration of energy exchange during charge and discharge, and is the product of coulombic and voltaic efficiencies:

$$\eta_e = \frac{E_{discharge}}{E_{charge}} = \frac{\overline{VI\Delta t}_{discharge}}{\overline{VI\Delta t}_{charge}} = \eta_c \eta_V$$

Energy efficiency is comprehensive of all the VRFB phenomena, it is no affective in highlighting the kinetics contribution to the efficiency.

Another important parameter to evaluate is the electrolyte utilization, this value gives information about the real utilized capacity respect the maximum theoretical capacitance.

Electrolyte utilization is related to the Depth of Discharge (DOD) an important parameter for Redox flow battery system design, define as:

$$DOD = SOC_{max} - SOC_{min}$$

Since the maximum theoretical SOC is obtained when maximum theoretical capacitance is reached the aiming of the DOD should be 100%, discrepancies from theory rise from overpotential and the imposed CUT-OFF in order to prevent side reaction. Overpotentials are responsible to increase (for charge) and decrease (discharge) the cell's energy from the equilibrium one described by the Nernst equation. The cell stops to charge/discharge before the effective achievement of the maximum theoretical work, leading to a lower $SOC_{max/min}$. On a discharge cycle, the quantity of electron produce is equal to the difference between the starting SOC and the final SOC.

$$electrolite\ utilization = \frac{i\ A\ \Delta t}{V\ c_0\ z\ F} = \frac{i\ A\ \Delta t}{x\ z\ F} = \frac{SOC_{start} - SOC_{end}}{SOC_{\max th.}}$$
$$= \frac{SOC_{start}}{SOC_{\max th.}} - \frac{SOC_{end}}{SOC_{\max th.}} = SOC_{max} - SOC_{min} = DOD$$

Where *i* is the current density, A the geometrical electrode area, Δt is the time for discharge, V is the volume of electrolyte, c_0 the nominal concentration, z the transfer charge and F is the Faraday constant.

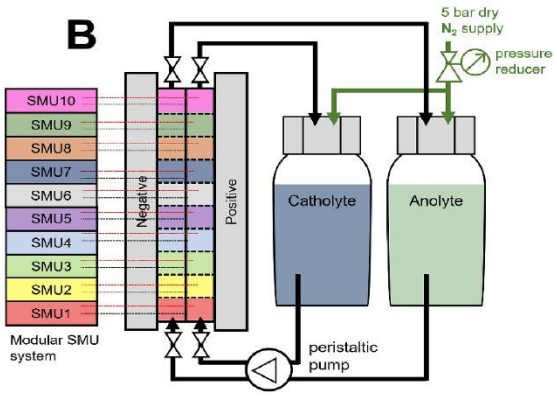

Figure 4.12: schematic view of a segmented flow battery full cell (figure taken from [60])

4.3.1 Experimental Data

For all the experiments membrane Nafion 115 is been used, this membrane has been choice for its high cross-over limitation despite the high ohmic resistivity (20mΩ). Cut off potential for charge and discharge cycle have been set at 1.8V and 1.1V respectively in order to deny secondary reaction such as HER and carbon corrosion. In figure 4.13 are plotted the voltaic efficiency and voltaic efficiency iR corrected of the full cell tested at different current densities.

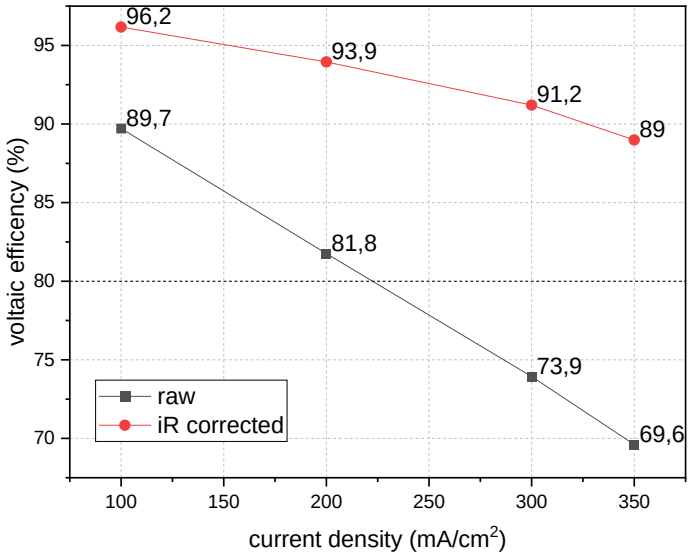

Figure 4.13: voltaic efficiency at different current densities

This result has been taken from the whole cell area of 25cm^2, performance and efficiencies are also influenced by the cell geometry that affect the mass transport of electrolyte inside the electrode, moreover the electrode has a nominal thickness of 300 um. Same result have been obtain from Zhao et al [56] with a cell area of 4cm^2, an electrode with 6mm nominal thickness and a Nafion 211 membrane that is a thinner membrane (50µm) with negligible ohmic resistance but higher cross-over phenome, this kind of membrane is not suitable for a cell set-up as used in this work because of the high cell area and hence higher cross-over due to the high exchange area over the membrane, in a geometry cell of 4cm^2 the cross-over at high current density are found to be negligible.

In figure 4.14 are plot the energy efficiency, raw energy efficiency has been calculated by the ratio of energy exchange during discharge over charge cycle, while the iR corrected energy efficiency has been estimated by multiplying the coulombic efficiency and the iR corrected voltaic efficiency. The iR corrected energy efficiency follows the same trend of the coulombic efficiency.

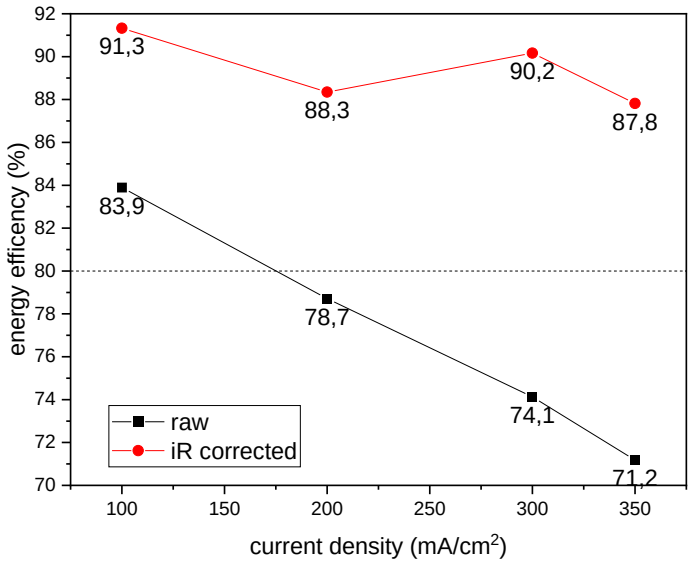

Figure 4.14: energy efficiency at different current densities

The current density at which the cell work is an average value over all the electrode, this mean that a part of the electrode can provide a current density slightly higher than the mean value, by using of the segmented cell is possible to ideally separate each part of the electrode and so isolate each polarization curve over the electrode area, from inlet to outlet, in order to analyze how the performance changes along the flow field. By this technique is possible to individuate the most performance area of the electrode and calculate the efficiencies (fig 4.15). For the serpentine flow field set-up, the most performative part just ahead the inlet. The inlet part is partially cover with the gasket for leakage reasons and so the performance in this section is hindered. In figure 4.16 are plotted the voltaic efficiencies of the whole cell and efficiencies of the inlet part.

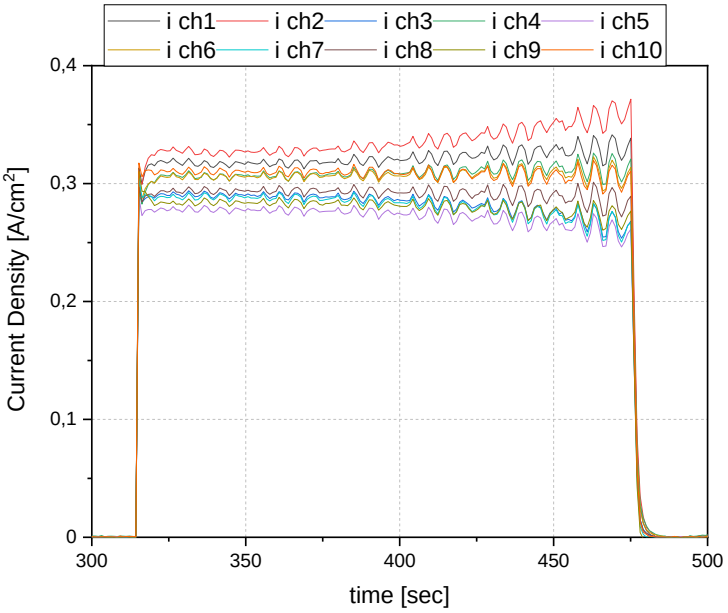

Figure 4.15: discharge cycle current density at different part of the segmented cell, mean value of 0,3A/cm^2

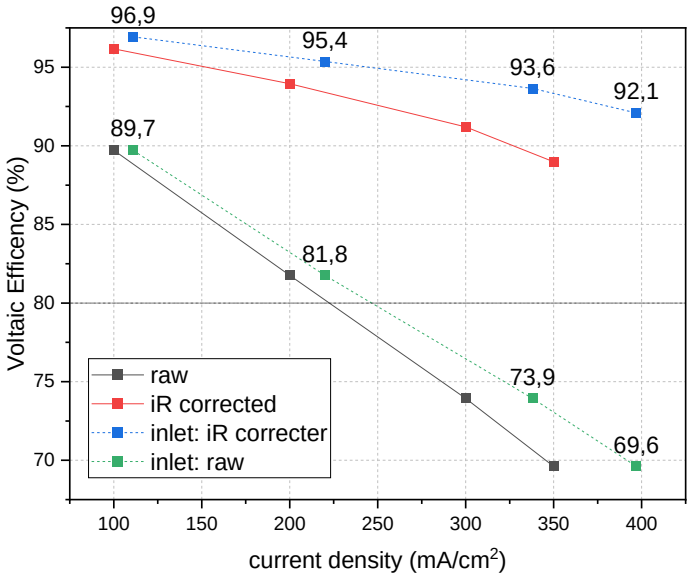

Figure 4.16: voltaic efficiencies at different current density, inlet sector efficiencies are dashed

As mentioned before, the inlet zone work at a higher current density than the mean cell and so the efficiencies are plotted against the current density measure in this sector. Analysis of the voltaic efficiencies at the inlet part of (2.5cm^2) present a value of 92% at 459mA/cm^2, the reasons for an higher prowess at the inlet are the presence of fresh reagent coming from

the tank and a lower pressure drop due to the flow field. At the inlet part the membrane overpotential get affected by the higher current density leading to a higher iR correction contribution.

Mainly due to the presence of carbon allotrope rather than nitrogen or oxygen the nano-material increase the index of merit of the VRFB, the usage of carbon paper 39AA rather than 29AA lead to a better performance with the serpentine flow field instead of interdigitate, mainly due to a larger thickness of the carbon fiber and promotion of larger mesoporousity that help the percolation of the electrolyte.

Study on degradation and stability of the electrode is out of the scope of this thesis work.

Chapter 5
Preliminary Techno-Economic Assessment

5.1 Design of a stationary VRFB 20MW & 160MWh

For this preliminary techno-economic assessment same assumption of [29] are considered in order to maintain unvaried most of the parameter and focus the attention on how the electrode could affect techno-economic assessment of a VRFB. In figure 5.1 is shown the cell average voltage at SOC 50% and the relative power density of the cell in charge and discharge, exposing an OCV(50%) of 1,44V, in line with other work.

Lower electrode overpotential can be exploit in order to reach higher voltaic and energetic efficiency at the same current density and increasing the depth of discharge (DOD), this led to a better utilization of the electrolyte and thus in a lower energy subsystem costs.

Another way to exploiting the low electrode overpotential is to maximize the current production over the battery, maintaining an energy and voltaic efficiency of ~80% and same DOD, in this case the economic gain is in the power subsystem costs, lowering the stack dimension and number of cell needed to reach a target power value. DOD have an high impact factore on the energy system design, value of DOD are obtain from litterature and are not necessarly coherent with the one from laboratory tests.

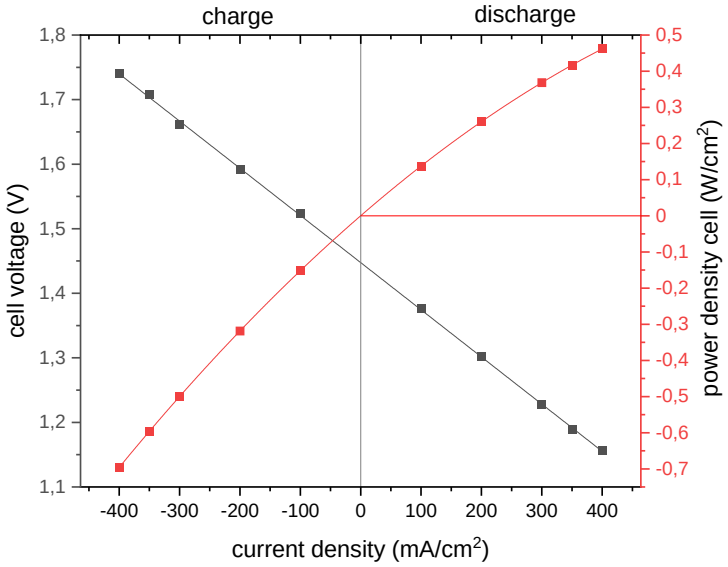

Figure 5.1: cell voltage and power density at SOC 50%

For the first assessment, where the main goal is saving from energy subsystem costs, current density of 100mA/cm2 has been considered, cell voltage value in charge and discharge are taken from experimental data, voltaic efficiency is calculated 90% and coulombic efficiency is assumed 99%, with those value a DOD of 0,8 (SOCmax 0,9; SOCmin 0,1) is considered for the assessment. A value of 2,7m^2 as cell area and Nafion 117 are considered in all the assessments. The cell power is equal to the product of cell voltage and current, which is the product of current density and active cell area, as shown in equation, in this case the cell power is taken from experiment data considering a cell area of 2,7m^2.

$$P_{cell} = V_{cell} \cdot i \cdot A_{cell}$$

Corresponding cell powers are $|P_{cell,\ charge}|$ = 4,1 kW and P_{cell} = 3,7kW. The total active cell area A can be calculated subsequently combining the power *P*, the cell voltage *V* and the current density *i*:

$$A = \frac{P}{V \cdot i}$$

For an plant power of 20MW a total active area of 14,6E^3 m^2 is calculated. The total number of cells n equals the quotient of total active cell area and active area of a single cell, the result is 5400 cells. It is assumed that the power subsystem is built modular, consisting of 250kW stack with n_{cell} = 68 cells each. On this basis the number of specific stack components is determined as follow. The number of membranes is equal to the number of cells, the domain of electrodes and gasket is double with respect to the number of cells, while the number of bipolar plates are equal to the sum of cells and stacks. Each stack requires two current collector and a stack frame.

Cost for membrane, electrode, bipolar plates and gasket are taken per meter squared and are value as in table 5.1.

Component	**Material**	**Thickness**	**Specific cost**	**Unit**
Membrane	Nafion 117	183 um	400	€/m^2
Electrode	CP with CNP	300 um	200	€/m^2
Bipolar plate	PPG86	7 MM	200	€/m^2
Current collector	Copper	20mm	3000	€ per unit
Cell frame and gasket	PVC, FKM		200	€ per unit
Stack frame			21000	€ per unit
Stack assembly			20500	€ per unit
Converters etc.			20000000	€ per system
Cables	Copper		4000	€/MW
PCS			5000	€ per system
Variable cost per PCS			+2000000	€ per system

Table 5.1: power subsystem costs

Electrode in consideration is the one studied in this thesis work, a proper economic value is not yet available, so its value can be incorrect. With those assumption a subsystem power of C_{power}= 25.450.000 € with a cost for single stack of 190.350 € has been calculated.

The energy capacity of the VRFB system is proportional to the amount of electrolyte. The core component of the energy subsystem is therefore the vanadium electrolyte consisting of

vanadium ions, sulfuric acid and water. Additional components of the energy subsystem are the two tanks, pumps, pipelines and fittings and heat exchangers. These components are often listed as auxiliaries, but in the present approach all system components are assigned to either the power or the energy subsystem. In addition, the assembly of the subsystem is considered. Energy subsystem costs evaluation bring to a value of each electrolyte volume by the Faraday law of $3,4*10^3$ m^3 with a tank volume of $5,1*10^3$ m^3, multiplying those value by the costs per unit of volume give a value for each electrolyte cost of 15,3 million of € and each tank cost of 1,53 million of €, pipeline and pump costs are evaluate as 480.000€ and 10.000€ respectively, no consideration of heat exchange system have been made. Since in a VRFB system are present anolyte and catholyte the cost of electrolyte and tank have to be double. Sum of all the energy costs give a value for energy subsystem C_{energy} = 34.640.000 €.

Total system cost is simply given by the sum of energy and power subsystems cost as explained in section 1.5 of approximately C_{system} = 62 million of €.

In the second assessment the focus is to enhance the current density and thus decreasing the power density cost rather than the electrolyte consumption. For the sake of simplicity, the calculus are omitted in this case study the current density considered is about 200mA/cm^2, maintaining the same geometry cell, DOD of 0,6 and voltaic efficiency of 80%, the value of cell voltage are still taken by experiment value. With this set-up each cell delivers a power of P_{cell} = 7,02kW. With this power only 2850m^2 of active area is require obtaining an plant of 20MW, each stack are building modular with a stack power of 250 kW, number of cells for each stack is 30. This set-up decrease notably the stack size and thus all the cost related to the stack assembly and stack components. Full power subsystem costs is about C_{power} = 9.500.000 €. To maintain the same discharge time, increasing the discharge rate a larger electrolyte volume is required and thus cost on energy subsystem have been calculated around C_{energy} = 43.200.000. summing the subsystems cost a total cost for an plant of 20MW, 160MWh is around C_{system} = 54.700.000 €.

Since the reference plant system cost is of 81.900.000€ the introduction of the carbon nanostructured carbon paper electrode, give to an approximatively cost of the entire plant of about 75%. By decreasing the plant costs, vanadium flow battery plant could be competitive with the lithium-ion plant, where the cost per kWh is attested around 170 €/kWh, while this assessment gives a value around 390 €/kWh.

5.2 Domestic VRFB Assessment

Comparison of a VRFB domestic power plant produce by VoltStorage, namely "VoltStorage SMART" but with the introduction of the electrodes made in this thesis work is possible by looking at the technical datasheet provided by the manufacturer [61]. On the datasheet no information on number of cells, active cell area and ionic exchange membrane are given, the only information are the nominal power (800W), nominal tension (25,2V), max capacity (245Ah) and nominal energy (6,2kWh), beside this information on coulombic and energy efficiency (98% and 84% respectively) are provided. From those information, in particular from nominal power and nominal energy is possible to calculate the time of discharge (7,75h), from this information on nominal current value is obtainable from the maximum capacity, given a value of current of (31,6 A).

For the introduction of the nanostructured carbon electrode, and a good comparison of data, assumption on same energy and coulombic efficiency must be taken into account, in this case, following the data in figure 4.13 the choice fall in an electrode current density of 200mA/cm^2, in figure 5.1 is given the correspondent power density that is approximately 0,25W/cm^2, the cell average voltage at this parameters is considered 1,3V.

Since cell voltage depend on the Nernst equation, for delivery of 25,2V nominal tension, series connection between cells are considered, by series connection the generated current remain constant over the cells but the tension of the stack is given by the sum of each cell voltage. In this case the number of cell to be stack in series are given by division of the total voltage by the single cell voltage.

$$n_{cell} = \frac{25{,}2\ V}{1{,}3\ V} = 19{,}38\ \approx 20$$

Dividing the nominal power by the power density given total active area can be found.

$$A_{tot} = \frac{800\ W}{0{,}25\ \frac{W}{cm^2}} = 3200\ cm^2$$

The cell area can thus be calculated by dividing the total area by the number of cell.

$$A_{cell} = \frac{3200\ cm^2}{20} = 160\ cm^2$$

Each cell can dispense a total current given by the multiplication of the cell area and the current density.

$$I_{cell} = I_{tot} = 0{,}2\frac{A}{cm^2}\ x\ 160\ cm^2 = 32\ A$$

Current value is approximatively equal to the one given on the technical datasheet. Cell geometry can easily be taken as square so the total cell geometry introducing nanostructured carbon electrode is (12,65 cm x 12,65 cm).

Chapter 6
Conclusion

The work presented in this thesis has been developed at the Center for Nano Science and Technology, Istituto Italiano di Tecnologia. Mesoporous nanostructured films made of carbon nanoparticles for vanadium flow batteries application have been synthesized using NanoJeD, a novel PECVD source. The deposition method used permit to decouple the contribution given by the various component of the treatment, providing a fine-tuning of all the steps of the process.

Mesoporous films have been characterized from physical, morphological and electrochemical point of view in order to relate how the various process step affect the material properties. The material as deposited is a hydrogen enrich carbon-based nanoparticle assembled film, Raman characterization shown that the carbon hybridization is prevalently sp^3 explaining the low conductivity and so the scarce performance as electrode. Thermal treatment has been demonstrate efficient in increasing the conductivity of the material, during annealing procedure pyrolization of the carbon-hydrogen film lead to releasing of hydrogen and subsequently reorganization of carbon from an sp^3 tetrahedral coordination to an sp^2 graphite-like carbon, increasing conductivity and crystallinity level, in this work temperature ranging from 800°C to 1100°C have been performed. Annealing procedure is known to reduce the film thickness and produce a densification of the material, by a sintering process [33] [32]. SEM analysis of the cross-sectioned films after various temperature of annealing shown a different trend, the thermal treatment is attend at high vacuum pressure (10^{-3}Pa), sintering process occur at pressure higher than the ambient one, to confirm this assumption BET and density analysis should be perform.

Morphological and chemical analysis performed by the means of Raman and XPS shown that during the thermal treatment a graphitization process occur, the Raman fitting procedure, with a bottom-up approach, suggest that the carbon material annealed at 800°C

consist in a simple graphitic carbon structure with presence of hydrogen, while the presence of carbon allotropes rising from annealing temperature higher than 900°C. XPS analysis prove the presence of heteroatom inside the deposited film, in particular Oxygen and Nitrogen carbon bonded, the presence of this molecules is the result of contaminant presence on the deposition or annealing procedure: in particular Nitrogen-doped carbon nanoparticles should rise from plasma reaction, air presence during the deposition process is the best suitable answer to their introduction. Nitrogen and Oxygen content decrease with the increase of the annealing temperature while the carbon allotropes presence are confirm from the XPS and their relative concentration increase with the temperature until reaching a plateau at around 1000°C where the relative concentration of carbon allotropes is of 57%. For identification of which carbon allotropes is present on the material a HRTEM analysis has been already required.

Electrochemical analysis procedure imposed to the sample comprise of CV, Symmetrical cell test and Full cell test. CV results show that the best performance as peak separation (spread) and peak ration is achieved with the electrode annealed at 1000°C. The material has been deposited on Glassy Carbon substrate and the faced electrode surface has been mask in order to identify a known exposure area. Annealing temperature of 1000°C bring the material to the lowest density and higher thickness, this reflect the porosity of the material and hence the superficial specific area, this together with the highest presence of carbon allotropes could explain the best performance achieve by this electrode. Symmetrical cell analysis have been performed in order to measure the overpotential produce by the electrode during the redox reaction of V^{2+}/V^{3+} at different testing condition such as fluid velocity and flow-field geometry, even in this test the best performance has been achieve from the electrode annealed at 1000°C, the possible answer to explain such a low overpotential could be found on the higher porosity, higher exposed surface and major intrinsic active catalytic point due to the higher presence of carbon allotropes and deflection of graphite plane rather than the presence of nitrogen and oxygen dopant that even if is demonstrate that those dopant are effective to increase the catalytic activity toward Vanadium redox reaction. Full cell VRFB has been tested only with the best resulting electrode from the previous analysis. In this test cell parameter efficiency as voltaic, energetic efficiency and electrolyte utilization has been calculated, the VRFB with this mesoporous carbon nanostructure electrode has been tested with a Nafion 115 membrane and 50mL of electrolyte tanks. Results shown an incredible high voltaic efficiency, especially if the ohmic loss due to the membrane is subtracted. Electrolyte utilization are instead low values, this could be due to the low electrolyte volume and to the high membrane overpotential.

My thesis work end with a preliminary techno-economic assessment of an stationary energy storage VRFB of 20MW and 160MWh, the assessment is done taking as reference the work done by [27] [29], almost of the parameter are kept the same in order to highlight the influence that the electrode has over the entire system. Techno-economic assessment shown that by introducing mesoporous electrode produced in this thesis in a VRFB plant for grid energy storage the system cost could be reduced by 25%.

6.1 State of art comparison

Data comparison with the published state of art is not trivial because there is no established standard testing procedure. System component and testing parameter contribute a lot to the cycle efficiency. Concerning component system almost all the element affects VRFB index of merit: thickness membrane, flow field, electrode morphology, cell area and electrolyte concentration. For the system parameter as example is reporter the cut-off potential: having a wider spread voltage region between superior and inferior cut off the voltaic efficiency value, defined as the ration between the average charge-discharge voltage, get penalized, while it allow to increase the reaction time and so the ΔSOC exploited during the cycle, increasing electrolyte utilization. In literature there is wide range of cut off employed, ranging from 1.7 to 1.8 V for the upper one and from 1.1 to even 0.7 for the lower.

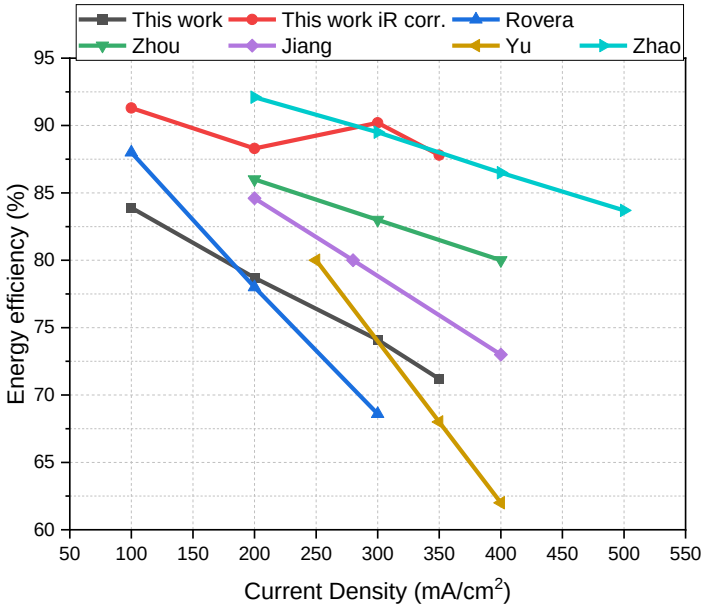

Figure 6.1: State of Art of VRFB

Author	Cell Area [cm^2]	Flow Rate [mL/min]	Nafion Thickness [µm]	Molarity [M]	Cut-off [V]
This work	25	100	127	1	1,8-1,1
Rovera [32]	25	100	127	1	1,8-1,1
Zhou [62]	4	900	50	1	1,65-0,8
Jiang [63]	4	45	50	1	1,6-0,8
Zhao [15]	4	80	50	1,1	1,65-1
Yu [64]	25	Not declare	50	1,5	1,65-0,8

Table 6.1: State of Art of VRFB

Another important affecting parameter is the flow field distributor and electrode coupling, since each distributor coupled with paper or felts shown different performance, this may lead to an undistinguishable of mass transfer phenomena from kinetic properties. Moreover, cell geometry effect the fluid dynamics generating different heterogeneities across the electrode and thus different mass transport problem, complicating the comparison between different cells.

In figure 6.1 are reported the more recent works with electrode's treatments and the works presented by the precedent co-worker at the NanoJeD system deposition, for what state before is not possible to identify a best overall electrode. Furthermore, no indication on degradation or electrode stability is considered in this work.

6.2 Future Perspective Work

Further improvements are possible by lowering the membrane overpotential, leading to higher electrode current densities, power densities without experiencing side reaction reactions. In figure 6.2 are shown the average cell potential and the power densities without the membrane overpotential contribution. In this case a voltaic efficiency of 88% with a current density of 400mA/cm^2 can lead a 1,3m^2 (1100 mm x 1100 mm) cell to deliver the same amount of power (7,02 kW) of the assessment in section 5.1, stack cost will drastically decrease and so the power subsystem costs, moreover by introduction of a smaller cell, cross-over contamination would also have a smaller impact, permitting to use a thinner membrane with lower resistivity.

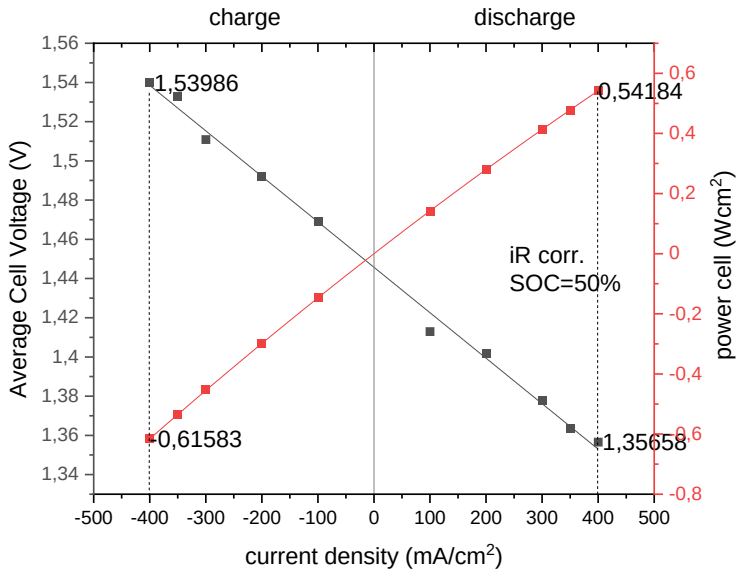

Figure 6.2: average cell voltage and relative power density at different current densities, iR correction and SOC 50% assumption

Another possible way to increase the current density and cell power is to stack different layer of carbon paper in order to increase the total thickness and active surface of the whole electrode, this solution will also increase the electrodes overpotential, so a trade-off for thickness over cell voltage and cell power must be found, J. Houser at al. [65] already tested the effect that stacking different carbon paper electrodes has in the VRFB performance, he demonstrate that increasing electrode thickness by stacking different layer of carbon paper 10AA discrepancies between different flow field start to be negligible, in his work the best performance with one electrode is obtain with the interdigitated flow field.

Rather than membrane improvement or engineer solution modifying electrode assembly, another way to increase the affordability of VRFB is to further enhance the single electrode performance. To increase the affinity of the electrode to vanadium redox reaction introduction of a well-known concentration of dopant as Bi nanoparticle or oxygen/nitrogen group can be afford. Metallic nanoparticles could be introduced in the material by the means of the ALD present in the CNST. Furthermore, a new method of thermal treatment, in order to decrease the production costs can be explore, as example rapid thermal annealing permit to reach higher temperature than the ones in this thesis work, with a lower consumption of energy in term of electricity and time of annealing. The possibility to reach higher

temperature is not necessary cause the carbon allotropes relative concentration seem to reach a plateau at 1000°C. lowering the production time of an electrode, in an industrial scale lead to reduction of the single component.

On the material procedure side, in the future, for a major control on the film uniformity and particle size, a modification of the diffusor inside the NanoJeD system should be done, diffusor in particular manage the ingress of gas inside the rection chamber, defining the resident time and wide of path. Inside the reaction chamber most of the peculiarity of the produced material are formed since the deposition chamber define only the landing mode.

Moreover, a stability test on the material should be performed in order to assess the chemical and mechanical stability of the nanoparticles attached to the substrate, degradation test could be perform by charge-discharge cycle test increasing the number of cycle, refill of the electrolyte could be necessary in order to eliminate the cross-over related issues.

Bibliography

[1] «project europe 2050,» [Online].

[2] T. Liu, X. Li, H. Zhang e J. Chen, «Progress on the electrode materials toward vanadium flow batteries (VFBs) with improved power density,» *Journal of Energy Chemistry*, vol. 27, pp. 1292-1303, 2018.

[3] C. Minke e T. Turek, «Materials, system design and modelling approaches in techno economic assessment of all-vanadium flow batteries- A review,» *Journal of Power Sources*, vol. 376, pp. 66-81, 2018.

[4] C. A. V. a. B. Scrosati, «Modern batteries - An introduction to electrochemical power sources,» *Butterworth-Heinemann*, vol. 2nd edition, 1997.

[5] E. Gileadi, E. Kirowa, Eisner e J. Penciner, interfacial electrochemistry, ADDISON-WESLEY, 1975.

[6] wei, G., Liu, Zhao, H. & Yan e C., «Electrospun carbon nanofibres as electrode material toward VO2+/VO2+ redox couple for vanadium flow battery,» *Journal of Power Sources*, n. 241, pp. 709-717, 2013.

[7] P. Nir, D. G. Kwabi, T. Carney, R. M. Darling, M. L. Perry e Y. Shao-Horn, «Influence of edge- and basal-plane sites on the vanadium redox kinetics for flow batteries,» *the journal of physical chemistry*, 2015.

[8] Taylor, S. M. Taylor, A. Patru, D. Perego, E. Fabbri e T. J. Schmidt, «influence of carbon material properties on activity stabilityof the negative electrode in vanadium redox flow batteries: a model electrode study,» *applied energy material*, 2018.

[9] G. W. e. al., «Electrocatalytic effect of the edge planes sites graphite electrode on the vanadium redox couple,» *Electrochimica Acta*, n. 204, pp. 263-269, 2016.

[10] N. P. e. al., «influence of edge and basal plane site on the vanadium redox kinetics for flow batteries,» *journal of physical chemistry,* n. 119, pp. 5311-5318, 2015.

[11] l. wei, t. zhao, zeng, x. zhou e y. zeng, «Copper nanoparticle-deposited graphite felt electrodes for all vanadium redox flow battery,» *applied energy,* n. 180, pp. 386-391, 2016.

[12] z. He, m. li, y. li, c. li, z. yi, j. zhu, l. dai, w. meng, h. zhou e l. wang, «ZrO2 nanoparticle embedded carbon nanofiber by electrospinning technique as advanced electrode material for vanadium redox flow battery,» *electrochimica acta,* n. 309, pp. 166-176, 2019.

[13] «methods to improve electrochemical reversibility at carbon electrodes,» *journal of electrochemical society,* n. 131, pp. 1578-1583, 1984.

[14] H. Jiang, W. shyy, M. Wu, R. Zhang e T. Zhao, «A bi-porous graphite felt electrode with enhanced surface area and catalytic activity for vanadium redox flow battery,» *Applied Energy,* n. 223-224, pp. 105-113, 2019.

[15] X. Zhou, Y. Zeng, X. Zhu e T. Zhao, «A high performance dual-scale porous electrode for vanadium redox flow batteries,» *Journal of Power Source,* n. 325, pp. 329-336, 2016.

[16] L. Xia, Q. Zhang, C. Wu, Y. Liu, M. Ding, J. Ye, Y. Cheng e C. Jia, «Graphene coated carbon felt as high-perfomance electrode for all vanadium redox flow batteries,» *Surface & Coating Technology,* n. 358, pp. 153-158, 2019.

[17] Y. Shi, C. Eze, B. Xiaong, W. He, H. Zhang, T. Lim, A. Ukil e J. Zhao, «Recent development of membrane for vanadium redox flow battery: A reviw,» *Applied Energy,* n. 238, pp. 202-224, 2019.

[18] C. a. E. E. w. t. Battery, «Battery university,» 2019. [Online]. Available: https://batteryuniversity.com/learn/article/bu_808c_coulombic_and_energy_efficiency_with_the_battery.

[19] M. Menictas e C. Kazacos, «Thermal stability of concentrated V(V) electrolytes in the Vanadium Redox Cell,» *journal of the Electrochemical Society ,* n. 143, pp. 86-88.

[20] F. Rahman e M. Skyllas-Kazacos, «Solubility of vanadul silfate in concentrated sulfuric acid solution,» *journal of power sources,* n. 72, pp. 105-110, 1998.

[21] L. Li e e. al., «A stable Vanadium Redox Flow Battery with high energy density for large-scale energy storage,» *Advance Energy materials,* n. 1, pp. 105-110, 1998.

[22] M. Skyllas-kazacos, C. Peng e M. Cheng, «Evaluation of precipitation inhibitors for supersaturated Vanadyl Electrolytes for the Vanadium Redox Battery,» *Electrochemical and solid state letters,* n. 2, pp. 121-122, 1999.

[23] A. Mousa e M. Skyllas-Kazacos, «Effect of additives on the Low-Temperature stability of Vanadium Redox Flow Battery Negative Half CEll Electrolyte,» *ChemElectroChem,* n. 2, pp. 1742-1751, 1999.

[24] L. Wei, T. Zhao, Q. Xu, X. Zhou e Z. Zhang, «In situ investigation of hydrogen evolution behaviour in vanadium flow batteries,» *Applied Energy,* n. 190, pp. 1112-1118, 2017.

[25] N. M. e. al., «Impact of corrosion conditionon carbon paper electrode morphology and the performance in vanadium redox flow battery,» *journal of the electrochemical society,* n. 166, pp. 353-363, 2019.

[26] H. Liu, Q. Xu e C. Yan, «On line mass spectrometry study of electrochemical corrosion of the graphite electrode for vanadium redox flow battery,» *Electrochemistry communication,* n. 28, pp. 58-62, 2012.

[27] C. Minke e T. Turek, «Material, system design and modelling approaches in techno-economic assessment of all-vanadium redox flow batteries - A review,» *Journal of power Source,* n. 376, pp. 66-81, 2018.

[28] L. Ming-Jia, Wei, Zhao, Xi, Chen e T. Wen-Quan, «Economic analysis of a new class of vanadium redox-flow battery for medium- and large-scale energy storage in commercial application with renewable energy,» *Applied Thermal Engineering,* n. 114, pp. 802-814, 2017.

[29] C. Minke, U. Kunz e T. Turek, «Techno-economic assessment of novel vanadium redox flow batteries with large-area cells».

[30] B. Zakeri e S. Syri, «Electrical energy storage system a comparative life cycle analysis,» *Renewable sustainable energy,* n. 42, pp. 569-596, 2015.

[31] M. Palmer, «Meet the startup building a sustainable alternative to Tesla’s Powerwall,» June 2020. [Online]. Available: https://sifted.eu/articles/voltstorage-tesla-powerwall-alternative/.

[32] E. Rovera, «Vertical integrated method for the development of carbo nano structured electrodes for vanadium redox flow battery,» Milano, 2019.

[33] C. Fasanotti, «Nanostructured carbon electrodes for vanadium redox flow batteries,» Milano, 2019.

[34] G. N. e. al., «Toward an electronic grade nanoparticle assembled silicon thin film by ballistic deposition at room temperature: the deposition method, structural and electronic properties,» 2018.

[35] M. Lieberman e A. Lichtenberg, discharge and material processing principle of plasma discharge and material, Wiley - Interscience, 2005, pp. 73-84.

[36] P. Chabert e N. Braithwaite, Physics of Radio-Frequency Plasmas, Cambridge University Press, 2011.

[37] C. Pattyn e e. al., «Nanoparticle formation in a low pressure argon/aniline RF plasma,» *Applied Physics letters,* 2018.

[38] K. U. e. al., «Generation and gworth of nanoparticles in low pressure plasma,» *Pure and Applied Chemistry,* 1999.

[39] G. Nava, *Nanoparticle Jet deposition. Anovel plasma-based approach for room-temperature, high-throughput an d large-are synthesis od nanostructured materials,* 2016.

[40] F. Sharipov e D. Kozak, «rarefied gas flow through a thin slit at an arbitrary pressure ratio,» *European journal of Mechanics,* n. 30, pp. 543-549, 2011.

[41] T. Kim, J. Lee e K. lee, «Full graphitization of amorphous carbon by microwave heating,» *RSC Advances,* vol. 6.

[42] C. Casiraghi, A. Ferrari e J. Robertson, «Raman spectroscopy of hydrogenated amorphous carbons,» *Physical review B,* vol. 72, 2005.

[43] S. Rodil, A. Ferrari, J. Robertson e S. Uhl, «Infrared spectra of carbon nitride films. Thin solid films,» *Internationa conerence on metallurgic coating thin film,* pp. 420-421, 122-131, 2002.

[44] S. R. e. al., «probing phonon dispersion relation of graphite by double resonance raman scattering,» *Physical review letters,* vol. 88, 2001.

[45] Y. Ko e et al., «onion-like carbon as dopant/modification-free electrocatalyst for VO2+/VO2+redox reaction: performance control mechanism,» *Carbon,* vol. 127, 2018.

[46] W. K. e. al., «The tribological of precursor molecules of fullerene-like hydrogenated carbon films under ionic liquid lubrication,» *Surface and interface analysis,* 2015.

[47] G. Y. e. al., «Resonant excitation of precursor molecules in improving the particle crystallinity, growth rate and optical limiting performance of carbo nano-onion».

[48] Z. G. e. al., «A reconsideration of the relationship between the crystalline size loaf carbon determined by X-Ray difraction and Raman spectroscopy,» *Carbon,* vol. 44, 2006.

[49] P. R. e Renishaw, «Renishaw: photoluminescence,» 2'2'. [Online]. Available: http://Renishaw.com/en/photoluminescence-explained.

[50] M. B. e e. al., «Photoluminescence and Raman spectroscopy in hydrogenated carbon film,» *IEEE transaction on magnetics,* 1997.

[51] A. Jorio e e. al., «Characterizing carbon nanotubes samples with resonance raman scattering,» *new journal of physics,* 2003.

[52] A. C. F. a. J. Robertson, «Interpretation of Raman spectra of disordered and amorphous carbon,» *Physical Review,* vol. B, n. 295, p. 14, 2000.

[53] B. Lesiak e e. al., *Applied surface science,* n. 452, pp. 223-231, 2018.

[54] J. Jin e e. al., «identifying the active site in nitrogen doped graphene for VO2+/VO2+ redox reaction,» *ACS nano,* n. 7, pp. 4764-4773.

[55] M. Messaggi, P. Canzi, R. Mereu, A. Baricci, F. Inzoli, A. Casalegno e M. Zago, «Analysis of flow field design on vanadium redox flow battery performance: Development of 3D computational fluid dynamic model and experimental validation».

[56] J. Jiang, L. Sun, M. Wei, W. Wu, Shyy e T. Zhao, «A high power density and long cycle life vanadium redox flow battery,» *Energy Storage Material,* n. 24, pp. 529-540, 2020.

[57] A. G.-E. K. T. T. Shinagawa, «Insight on Tafel slopes from a microkinetic analysis of aqueous electrocatalysis for energy conversion,» *Scientific report,* vol. 5, p. 13801, 2015.

[58] K. Zhang, J. Xiong, C. Yan e A. Tang, «In situ measurement of electrode kinetics in porous electrode for vanadium redox flow battery,» *Applied Energy,* n. 272, 2020.

[59] D. Aaron e e. al., «In Situ Kinetics Studies in All-Vanadium Redox Flow Batteries,» *ECS Electrochemistry Letters,* vol. 2, n. 3, 2013.

[60] M. Messaggi, C. Rabissi, C. Gambaro, L. Medab, A. Casalegno e M. Zago, «Investigation of vanadium redox flow batteries performance through locally resolved polarisation curves and impedance spectroscopy. Insight into the effects of electrolyte, flow field geometry and electrode thickness.,» 2019.

[61] C. Hamann, A. Hamnet e W. Vielstich, Electrochemistry, WILEY-VCH, 2007.

[62] X. L. Z. e. al, «A high-performance dual-scale porous electrode for vanadium redox flow batteries,» *journal of Power source*, vol. 325, pp. 329-336, 2016.

[63] «Higly efficient and ultra-stable boron-doped graphite felt electrodes for vanadium flow batteries,» *Journal of material chemistry*, vol. 6, n. 27, pp. 13244-13253, 2018.

[64] Yu, «P-doped electrode for vanadium flow battery with high-rate capability and all-climate adaptability,» *Journal of Energy Chemistry*, vol. 35, pp. 55-59, 2019.

[65] J. Houser, J. Clement, A. Pezeshki e M. M. Mench, «Influence of architecture and material properties on vanadium redox flow battery performance,» *Journal of Power Source*, vol. 302, pp. 369-377, 2016.

Ringraziamenti

I primi ringraziamenti sono verso i prof. Andrea e Matteo, che non solo hanno saputo trasmettere la loro passione attraverso l'insegnamento, ma si sono rivelate persone di Cuore, disponibili e cordiali, Loro calcano perfettamente l'idea che ho di Vincenti.

Poiché dietro ogni grande Progetto c'è sempre una grande idea, devo ringraziare Fabio, ideatore del progetto.

A tutti i colleghi dell'IIT che con i loro consigli e la loro esperienza hanno saputo aiutarmi, ed in particolare Riccardo, Stefano ed Eugenio che sono stati il jolly, l'asso nella manica, quando le soluzioni scarseggiavano.

Ma i ringraziamenti più dovuti sono verso la mia faglia Claudio, Catia e Davide, che hanno saputo in ogni modo alimentare la mia passione ed i miei sogni.

Verso la mia fidanzata Sveva, per la pazienza, la comprensione, l'amore e la pazienza ancora.

Verso i colleghi universitari, i "TMB", ed i miei coinquilini, che hanno colorato le giornate altrimenti grigie di studio.

In ultimo ringrazio tutti quelli che credono in me e anche tutti quelli che non ci credono, siete l'energia che alimenta il motore delle mie ambizioni.